

#### Contents lists available at ScienceDirect

# Petroleum Science

journal homepage: www.keaipublishing.com/en/journals/petroleum-science



# Original Paper

# Evidence for active generation and seepage of sub-salt natural gas/condensate blend in the east offshore Nile Delta, Egypt: Integrated geochemical, petrophysical and seismic attribute approaches



Mahmoud Leila a, b, \*, Ahmed A. Radwan c, Amir Ismail d, e, Emad A. Eysa f

- <sup>a</sup> Geology Department, Faculty of Science, Mansoura University, Mansoura 35516, Egypt
- <sup>b</sup> School of Mining and Geosciences, Nazarbayev University, Astana 010000, Kazakhstan
- <sup>c</sup> Department of Geology, Faculty of Science, Al-Azhar University, Assiut Branch, Assiut 71524, Egypt
- <sup>d</sup> Department of Geology, Faculty of Science, Helwan University, Cairo 11795, Egypt
- e Department of Physical and Environmental Sciences, Texas A&M University—Corpus Christi, 6300 Ocean Drive, Corpus Christi, TX, 78412, USA
- f Geology Department, Faculty of Science, Zagazig University, Zagazig 44519, Egypt

#### ARTICLE INFO

# Article history: Received 9 February 2023 Received in revised form 12 October 2024 Accepted 11 November 2024 Available online 13 November 2024

Edited by Teng Zhu

Keywords:
Petrophysical evaluation
Source rock
Hydrocarbon geochemistry
Biomarkers
Gas chimneys
Rock-typing

#### ABSTRACT

Offshore Nile Delta in Egypt represents an enormous hydrocarbon province with recent projected gas and condensate discoveries of more than 50 trillion cubic feet "TCF". Most of these occur in the post-salt hydrocarbon plays where biogenic gases are dominant. This study integrates organic geochemistry, seismic geomorphology and petrophysics in order to decipher the origin, and accumulation conditions of the wet gas/condensate blend in the Upper Miocene sub-salt Wakar Formation sandstones in Port Fouad Marine "PFM" Field, offshore Nile Delta. Hydrocarbon pay zones are scattered thin (<10 m) sandstones deposited in as turbiditic channel/levee complex facies. Spatial distribution of vertical gas chimneys (~2 km wide) rooting-down to the Messinian Rosetta salt is associated with the lateral pinching-out of the turbiditic sandstones. Organically-rich (total organic carbon "TOC" > 1 w.t.%, hydrogen index "HI" > 200 mgHC/gTOC) and mature ( $T_{\text{max}}$  > 430 °C, vitrinite reflectance "VR" > 0.6 %R<sub>0</sub>), source rocks are restricted to Upper Miocene Wakar and Oligo-Miocene Tineh formations. The latter contains more mature organofacies (up to  $1.2 \%R_0$ ) and type II/III kerogen, thereby demonstrating a good capability to generate wet gases. The studied gas is wet and has thermogenic origin with signs of secondary microbial alteration, whereas the condensate contains a mixture of marine and terrestrial input. Molecular biomarkers of the condensate, isotopic and molecular composition of the gas reveals a generation of condensate prior to gas expulsion from the source. The Wakar sandstones have a heterogeneous pore system where three reservoir rock types (RRTI, RRTII and RRTIII). RRTI rocks present the bulk composition of the Wakar pay zones. Spatial distribution of RRTI facies likely control the accumulation of the sub-salt hydrocarbons. Our results provide a new evidence on an active petroleum system in the sub-salt Paleogene successions in the offshore Nile Delta where concomitant generation of gas/condensate blend has been outlined.

© 2024 The Authors. Publishing services by Elsevier B.V. on behalf of KeAi Communications Co. Ltd. This is an open access article under the CC BY-NC-ND license (http://creativecommons.org/licenses/by-nc-nd/4.0/).

#### 1. Introduction

Petroleum source rocks are capable of generating and expelling both liquid and gaseous hydrocarbon phases (e.g. Tissot and Welte, 1984; Hunt, 1996; Whiticar, 1999; Peters et al., 2005). The source

E-mail address: mahmoud\_lotfy@mans.edu.eg (M. Leila).

rock characteristics (organic matter quality, quantity and maturity) control the type hydrocarbons generated (Peters and Cassa, 1994; Hunt, 1996; Leila and Moscariello, 2017; Abdelwahhab et al., 2022; Radwan et al., 2022b; El Matboly et al., 2022; Fathy et al., 2023). Concomitant generation of light liquid hydrocarbon and natural gas blend has been reported from different geological contexts around the globe (e.g. Leila and Moscariello, 2017; Loegering and Milkov, 2017; Leila et al., 2022a; Hassan et al., 2023a). Generation, expulsion and temporal evolution of these hydrocarbon phases are

<sup>\*</sup> Corresponding author. Geology Department, Faculty of Science, Mansoura University, Mansoura 35516, Egypt.

controlled by various geological processes (biogenesis versus thermogenesis and primary versus secondary cracking). Therefore, understanding the link between these processes and accurate deciphering of hydrocarbon origin are crucial for petroleum exploration and development campaign. Additionally, the accumulation versus seepage of the expulsed hydrocarbons depend on the spatial distribution of reservoir rock types (RRTs), migration paths as well as seal integrity (e.g. Leila et al., 2022b, c; Hassan et al., 2023b). Thus, delineating the active hydrocarbon kitchen and defining its link with RRTs distribution, and migration paths are essential for predicting the hydrocarbon accumulation as well as seepage zones.

With recent estimated discoveries of more than 50 trillion cubic feet "TCF", offshore Nile Delta presents one of the most promising regions for natural gas exploration in the world (Esestime et al., 2016). These gases have variable origin ranging from pure biogenic in some fields such as Zohr to thermogenic and mixed thermogenic-biogenic in other offshore fields (N. Baltim, Nouras) (Vandré et al., 2007; Esestime et al., 2016). Moreover, light oil and condensates were also reported from several offshore fields (e.g. Abu Qir, Temsah and Port Fouad Marine "PFM"). Commercial accumulation of these hydrocarbon phases is preliminary dependent on the presence of active feeding system (biogenic or thermogenic source) as well as effective compartment of potential reservoir and seal rocks (Peters and Cassa, 1994). The offshore Nile Delta presents an active region for subsurface gas seepage (e.g. gas chimneys) where sea-floor mud volcanoes were correlated with subsurface gas escape, thereby typifying presence of active feeding system with coupled with a reservoir or seal failure (e.g. Ismail et al., 2020, 2021, 2024). The studied PFM lies in the eastern offshore part of the Nile Delta (Fig. 1). It has been discovered in 1992 by the International Egyptian Oil Company (IEOC) and came on stream in April 1996 to initial production 70 MCF/d of gas and 3500 b/d of light oil. The Upper Miocene sandstones of Wakar Formation represent the main hydrocarbon reservoir in PFM wells (Fig. 2). Wakar sandstones represent an offshore equivalent for the Qawasim deltaic sediments that host very prolific reservoir targets in some onshore fields (e.g. Leila et al., 2020, 2023a). Gas chimneys were reported nearby the studied wells, therefore, PFM field provides an ideal region to investigate the controls on hydrocarbon generation, migration, and accumulation.

## 2. Geologic setting

The Nile Delta represents a large Paleogene-Neogene depositional system covering an area of approximately 250,000 km² in the northeastern part of the African continental margin (Fig. 1). The tectonic evolution of the Nile Delta started with the Neotethys opening associated with formation of an E-W flexure hinge zone separating the south delta stable platform from the mobile, subsiding north Nile Delta Basin (Fig. 1; Sestini, 1989; Said, 1990; Kamel et al., 1998; Dolson et al., 2005; Leila and Moscariello, 2019). Subsidence along the hinge zone faults triggered the deposition of a thick pile of Paleogene-Neogene sedimentary successions in the north Nile Delta Basin which host the most petroliferous stratigraphic horizons in the Nile Delta (e.g. Dolson et al., 2005; Nabawy and Shehata, 2015; Leila et al., 2020; El Adl et al., 2021).

Activation of old rift-fault trends (Temsah and Rosetta) fragmented the north Nile Delta basin into three sub-provinces or subbasins (Fig. 1; Sarhan and Hemdan, 1994; Bertello et al., 1996; Kamel et al., 1998). The study region lies in the southern part of the eastern sub-basin where the Temsah fault pattern is the main structural domain that controlled the depositional evolution of the Cenozoic sedimentary succession (Kamel et al., 1998; Lashin and Abd El-Aal, 2005). The area was influenced by inversion tectonics during the Paleogene subsequent to the Syrian arc phase, thereby the pre-Oligocene sedimentary succession has been extensively eroded (Mosconi et al., 1996; Hussein and Abd-Allah, 2001). The Oligocene sediments comprise thick succession of muddy turbidities accumulated contemporaneous to north-ward tilting of the Nile Delta where subaerial canyons delivered sediments from the Red Sea rift shoulders into the deep-water (Tineh Formation;

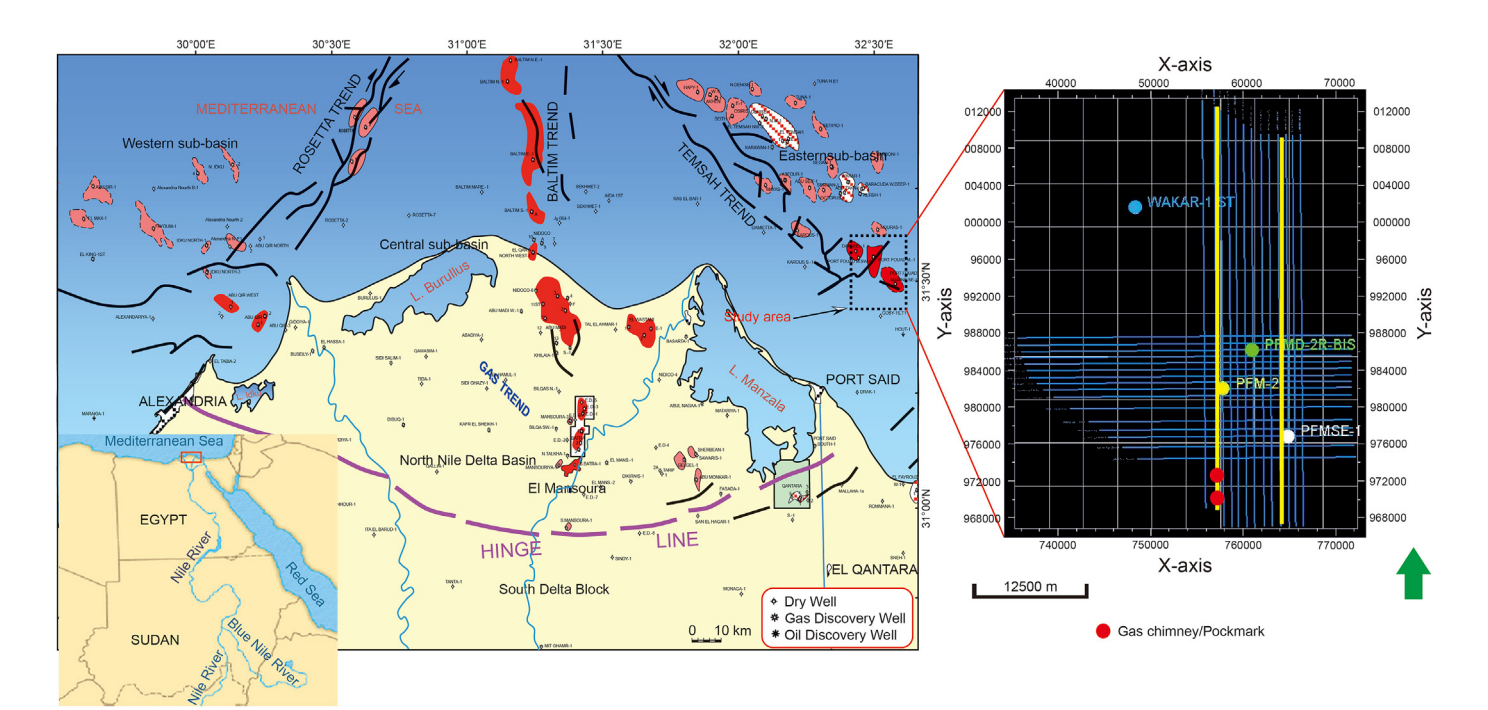


Fig. 1. Geologic map illustrating the location of the study region in the southern part of the eastern sub-basin, offshore Nile Delta. Yellow lines represent the seismic profiles shown in Figs. 3 and 4.

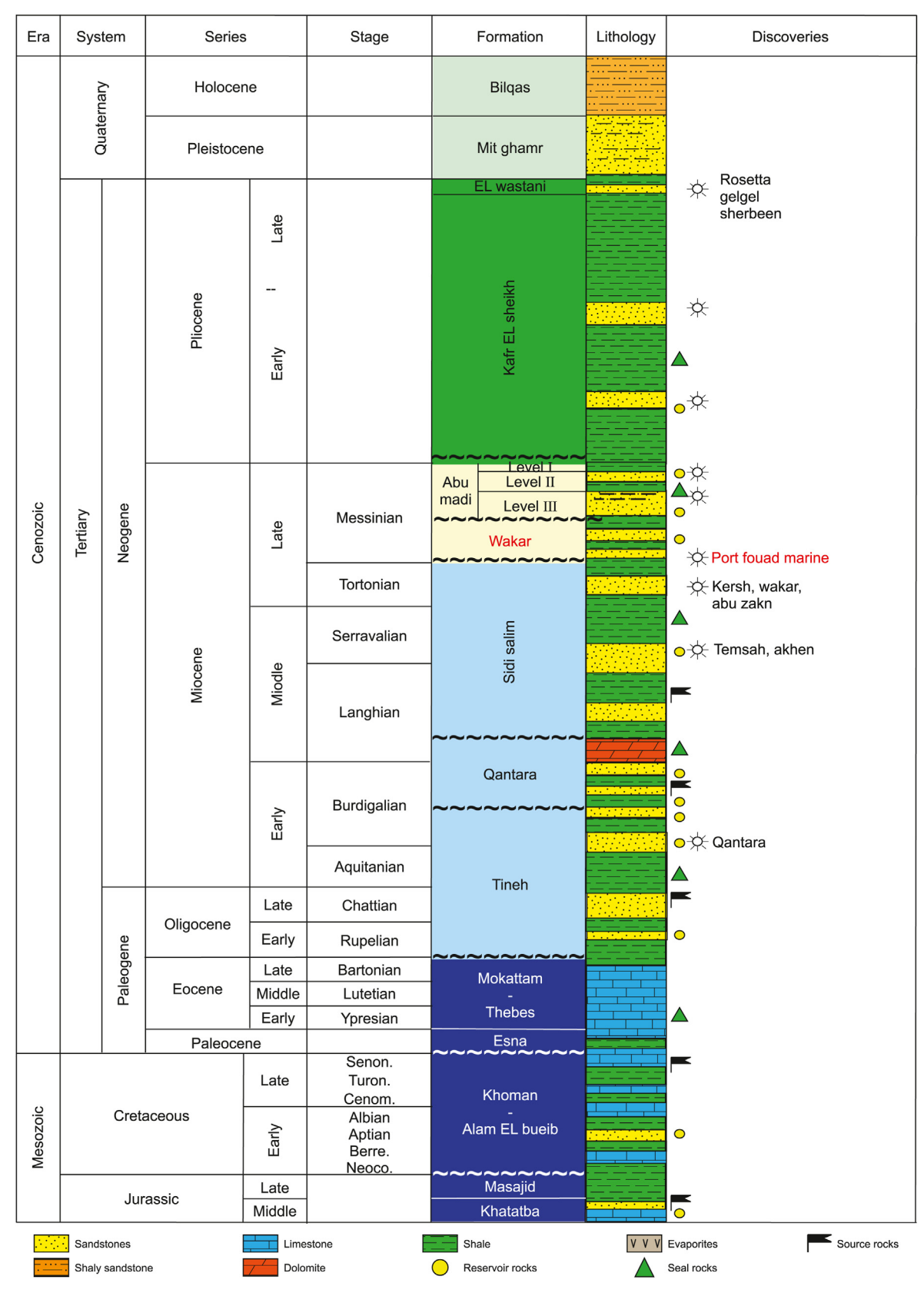


Fig. 2. Lithostratigraphic column of the Nile Delta eastern sub-basin illustrating the main source rock and reservoir intervals (modified after Leila and Mohamed, 2020).

#### Dolson et al., 2005).

The Neogene-Quaternary sedimentary succession in the eastern sub-basin was evolved during three different tectonostratigraphic cycles (Fig. 2; Rizzini et al., 1978). The youngest is the Miocene cycle which begins with a major transgressive episode resulting in accumulation of thick succession of open marine mudstones interbedded with deep-water carbonates. Large-scale sea level fluctuations prevailed during the deposition of the Middle and Upper Miocene strata, however, marine conditions prevailed throughout the Middle Miocene. Therefore, the marine mudstones and sandstones of the Sidi Salem Formation rest unconformably above the Lower Miocene marine mudstones of the Qantara Formation (Fig. 2). Regressive phase prevailed during Late Miocene and deltaic sedimentation during Late Tortonian-Early Messinian where the deltaic sediments of the Qawasim Formation accumulated onshore while Wakar Formation turbidities deposited in the offshore. Late Messinian witnessed a massive sea level drop and a partial to complete desiccation of the Mediterranean (Messinian salinity crisis "MSC") took place resulting in accumulation of evaporites in the deep basins with coeval fluvial incisions on the margins (Hsü et al., 1973; Clauzon, 1982; Dolson et al., 2005; Leila and Moscariello, 2019; Madof et al., 2019). The MSC was ended with a catastrophic reflooding of the Mediterranean during Early Pliocene and the entire Nile Delta was covered by marine shales (Kafr El-Sheikh Formation) (Leila and Moscariello, 2019; Leila and Mohamed, 2020).

#### 3. Data and methods

### 3.1. Seismic data interpretation

Seismic dataset comprises post-stack 2D seismic profiles covering the studied PFM Field. The seismic data is sampled every 4 ms (ms) and has a dominant frequency of 25 Hz with a frequency range between 5 and 65 Hz. Seismic data analysis started with improving the signal-to-noise ratio. Afterwards, deterministic wavelet extraction and seismic-well tying were performed to identify the actual seismic response of the stratigraphic horizons. Columnar disturbance in seismic data (poor data zones) were detected to define the hydrocarbon seepage zones and their associated features such as pockmarks, bright anomalies, and bottom-simulation reflectors (BSRs) (Hyndman and Spence, 1992; Sun et al., 2011; Ismail et al., 2021). Seismic attribute extraction techniques were applied in order to improve the recognition of seismic reflection features depending on the seismic waveform characteristics (Gammaldi et al., 2022; Ismail et al., 2020, 2022).

#### 3.2. Geochemical analyses

#### 3.2.1. TOC and Rock-Eval pyrolysis

Total organic carbon (*TOC*) and Rock-Eval pyrolysis measurements were carried out on 99 ditch cutting samples from two wells (PFMSE-1 and PMFD-2R) at StratoChem laboratories, Egypt. The selected samples cover all the studied successions: 48 samples from the Oligocene Tineh Formation, 30 samples from the Miocene Qantara and Wakar formations, as well as 21 cuttings from the Pliocene Kafr El-Sheikh Formation. The samples were crushed and washed with dichloromethane solvent to remove the hydrocarbon contaminants (oil base mud). *TOC* values in the studied samples were determined using a Leco CR12 system which involves a high temperature combusion ~1300 °C of the sample in the prescence of oxygen where the organic carbon will be released in the form of CO<sub>2</sub> which is then measured usin a solid state infrared detector. Rock-Eval pyrolysis analysis was performed using the Rock-Eval-6 appratus which comprises a programmed combusion of

60–70 mg of the sample in an inert atmosphere following the analytical procedure of Behar et al. (2001). The pyrolysis results include the organic carbon oxidation peaks  $S_1$ ,  $S_2$  and  $S_3$ . The first two parameters represent the amount of free and cracked hydrocarbon released during pyrolysis, respectively. The pyrolysis temperature at which  $S_2$  peak is obtained is the  $T_{\rm max}$  which infers on the thermal maturation level of the rock (Peters and Cassa, 1994; Hunt, 1996).  $S_3$  peak is the amount of organic  $CO_2$  released during pyrolysis at elevated temperature levels up to 550 °C.

#### 3.2.2. Vitrinite reflectance

Vitrinite reflectance ( $\%R_0$ ) measurements were carried out at StratoChem laboratories, Egypt on a total of 16 samples retrieved from Kafr El-Sheikh (n=9), Wakar (n=5) and Tineh (n=2) formations. A Zeiss Universal microscope system equipped with halogen, xenon, and tungsten was utilized to measure the reflectance intensity. Before measuring the reflectance, the samples were crushed and then seived using a 63  $\mu$ m seieve and then embedded in epoxy resin to prepare the thin sections. The reflecivity measurements were reported using a 546 nm wavelength monochromatic light following the analytical procedure of Mukhopadhyay (1992) and Peters et al. (2005). Reflectance measurements were reported only for the good quality vitrinite where the recycled and contaminated particles were excluded. A glass standard with a reflectance of 1.02% in oil were utilized in calibrating the apparatus prior to each measurement.

#### 3.2.3. Gas and condensate analysis

Gas analysis comprises the measurement of molecular and isotopic composition of three gas samples retrieved from the Wakar sandstones in PFMSE-1 (1 sample) and PFMD-2R (two samples) wells. Molecular composition of Wakar gases was obtained using a Hewlett Packard 5890 gas chromatograph equipped with a flame ionization detector (FID) which measures the different hydrocarbon gas phases. The abundant  $C_1-C_3$  gas phases were collected in order to measure their carbon isotopic composition ( $\delta^{13}$ C) using a Varian 3400 gas chromatograph equipped with an Isotope Ratio Mass Spectrometer (IRMS). Additionally, an upgraded Micromass 602 spectrometer was utilized to measure  $\delta D_{\text{methane}}$  following the procedure described by Sassen et al. (1999). The carbon isotope values were reported as parts per thousands (‰) relative to the Pee Dee Belemnite (PDB), while the deuterium isotope was measured relative to the Standard Mean Ocean Water (SMOW) with approximate experimental error (1 $\sigma$ ) of  $\pm 0.2\%$ .

Molecular biomarker analyses were conducted on one condensate sample retrieved from the Wakar sandstone reservoir in PFMSE-1 well. Saturates-aromatics and resin fractions were separated using a silica-alumina column chromatography. The carbon isotopic composition  $\delta^{13}C$  of saturates and aromatic fractions was measured using the Varian 3400 gas chromatograph-IRMS apparatus. Further chromatographic separation of the saturated fractions was performed and comprised a whole oil gas chromatography, and a detailed  $C_6$  &  $C_7$  gas chromatography to determine the relative concentrations of various molecular biomarkers. These analyses include a programed heating of the condensate sample from 40 °C to 340 °C with a temperature increasing rate of 10 °C/min following the analytical procedure described by Moldowan et al. (1984) and Peters and Moldowan (1993).

## 3.3. Wireline logging analysis

Complete suite of wireline logs retrieved from PFMSE-1 and PFMD-2R wells were interpreted to define the hydrocarbon pay zones and calculate their petrophysical properties. The calculated

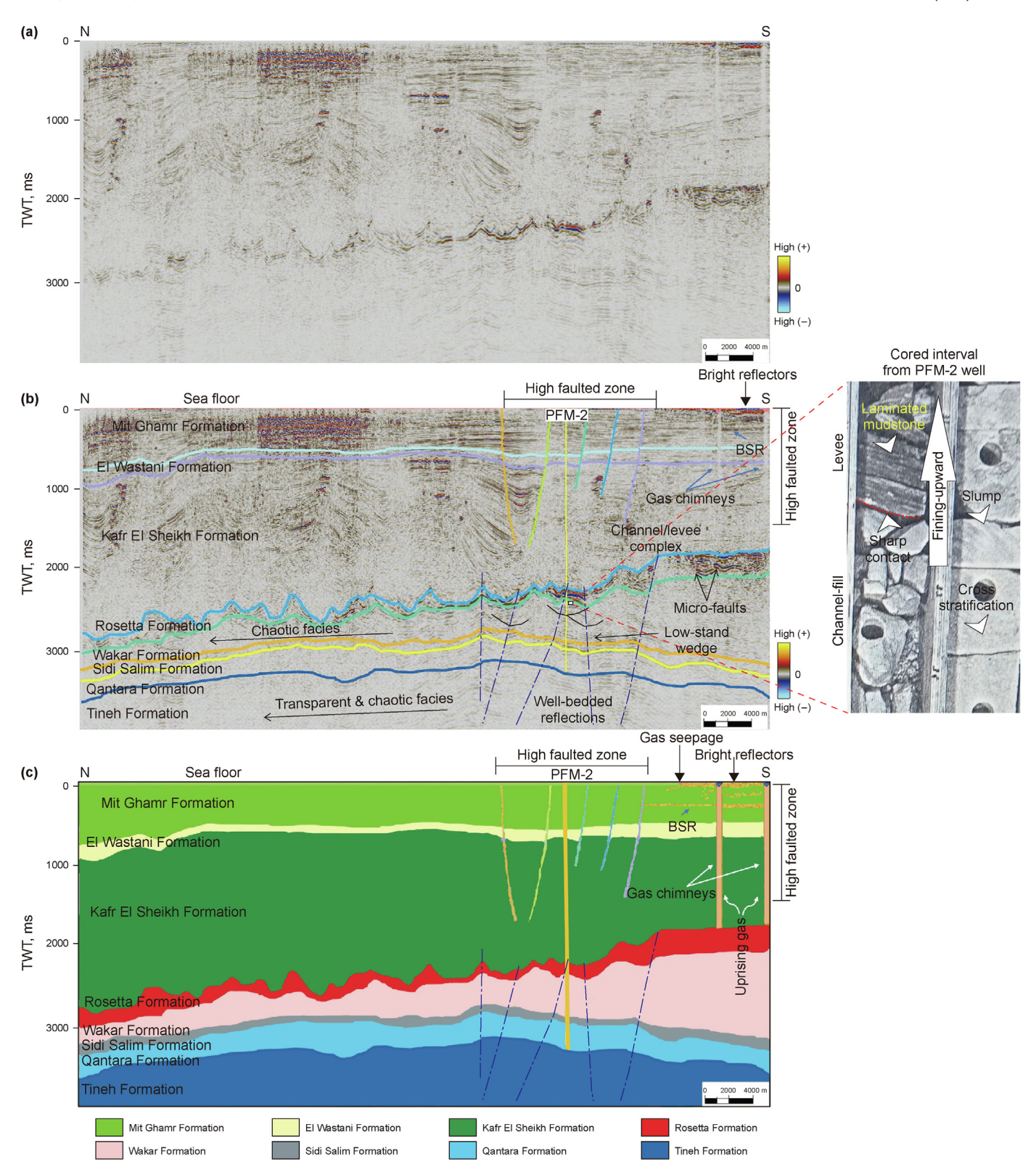


Fig. 3. (a) The original amplitude seismic; (b) An enhanced seismic section tied with PFMSE-1 well; (c) An interpreted 2D stratigraphic section illustrating a thinning of the Wakar Formation northward. The seismic profile location is shown in Fig. 1.

petrophysical parameters include total and effective porosity, shale volume, and water and hydrocarbon saturations. The standard petrophysical formation evaluation procedure was followed in this study (Poupon et al., 1970; Asquith and Gibson, 1982; Dewan, 1983;

Schlumberger, 1991; Abdelwahhab et al., 2022; Radwan et al. 2021, 2022a; Radwan and Nabawy, 2022). The formation water resistivity  $(R_{\rm w})$  and cementation factor (m) of the Wakar sandstones were determined using Pickett's plot (Pickett, 1972).

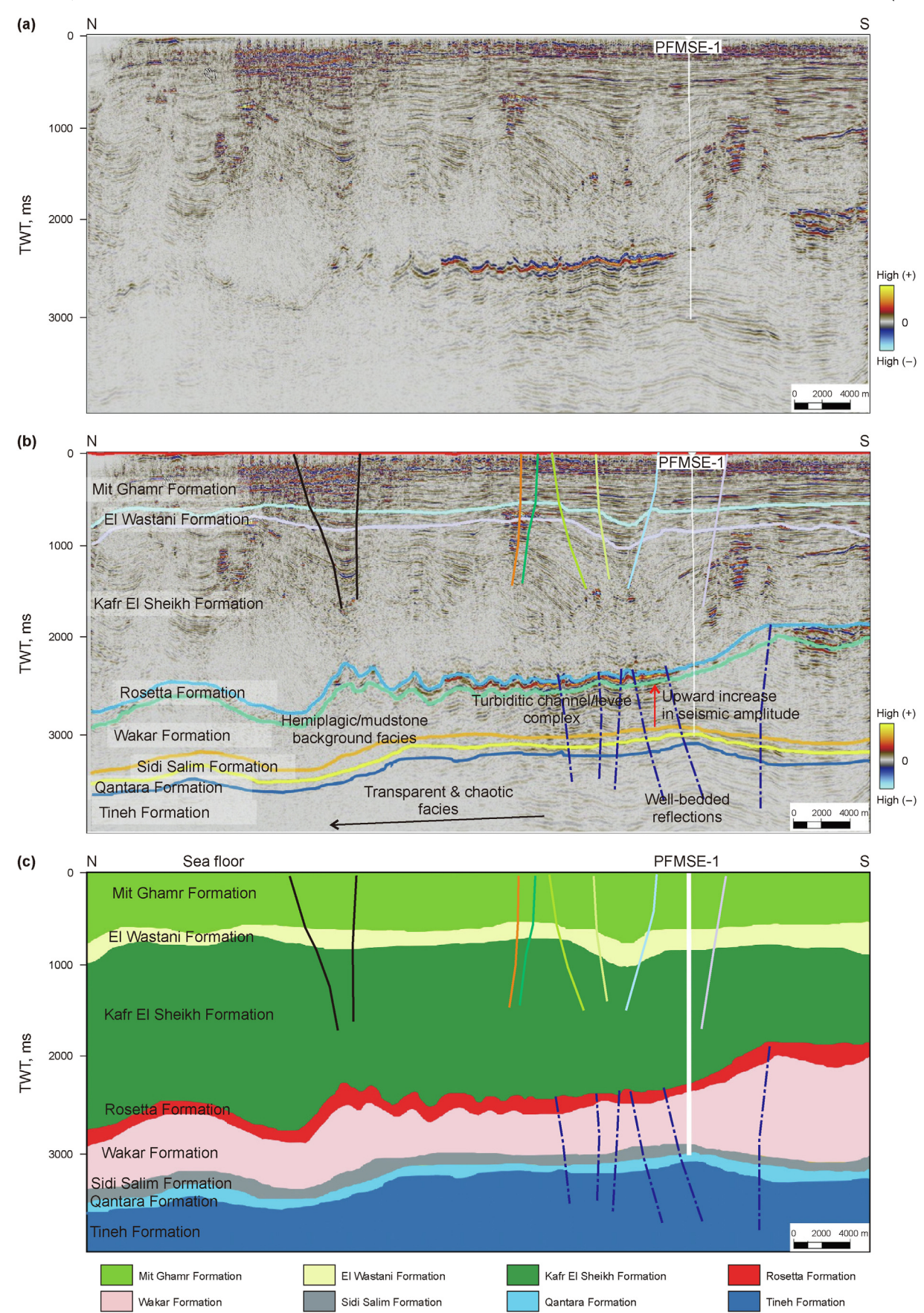
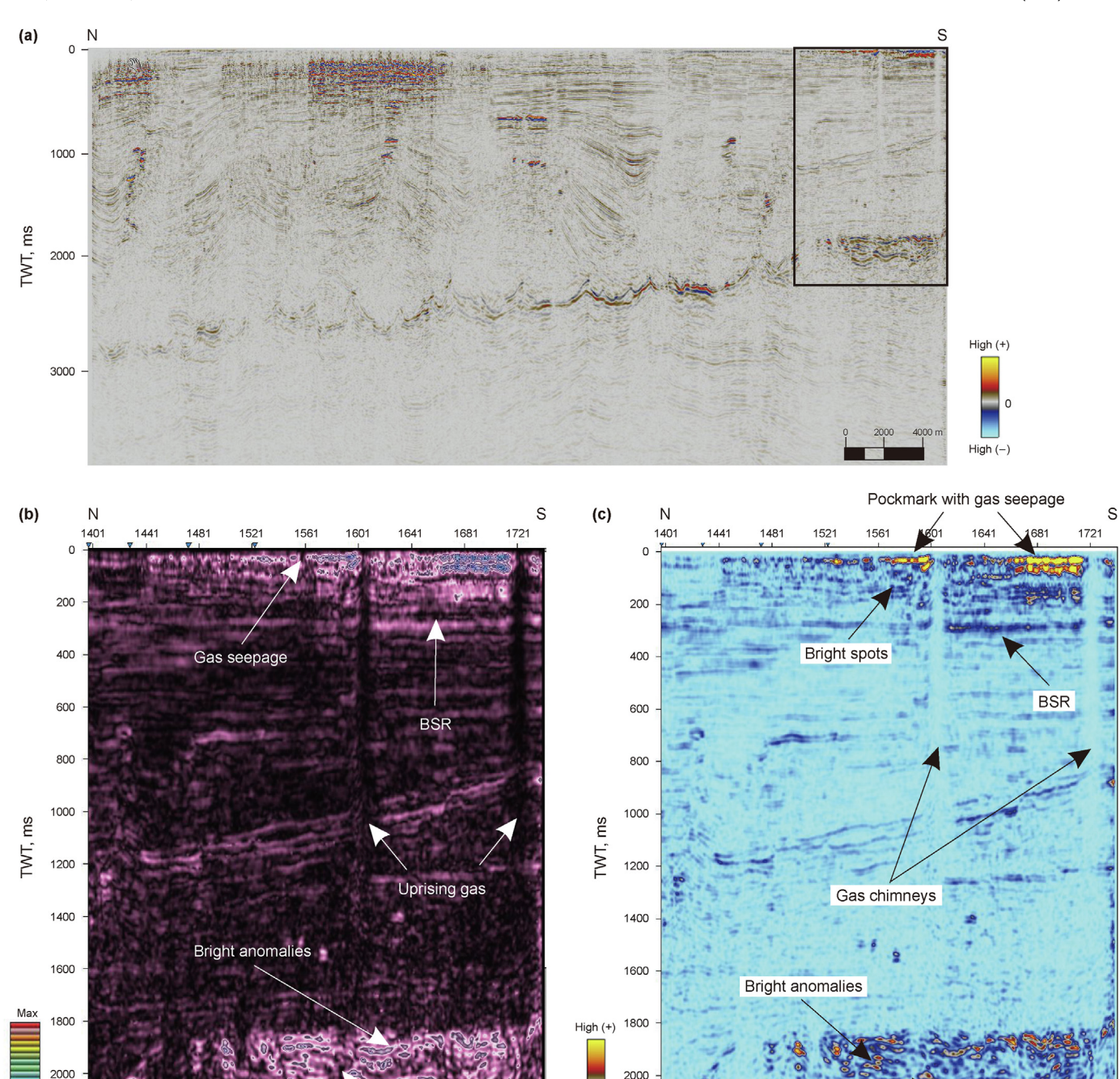


Fig. 4. (a) The original amplitude seismic section; (b) an enhanced seismic section; (c) an interpreted stratigraphic section demonstrates the lateral variation in thickness in the study region. Gas chimneys are clearly depicted in (b) and (c) as vertical gas pathways, shallow faults, BSR, and bright reflectors and anomalies. The seismic profile location is shown in Fig. 1.



**Fig. 5.** (a) The original amplitude seismic section illustrating some vertical discrepancies interpreted as gas seepage regions (see the black rectangle); sweetness and RMS attribute extraction (**b**, **c**) for the enlarged rectangle in (a) illustrating the bright anomalies, BSR, and bright reflections (besides the pockmarks) with the maximum values while the gas chimneys with minimum values.

High (-) 2200

# 3.4. Routine core analysis

Routine core analysis involves porosity, permeability, and grain density measurements for selected 22 core plugs from the Wakar sandstones in two wells (PMFD-2R and Wakar-1). These routine measurements were conduted in Corex laboratories, Egypt using helium gas expansion porosimieter and nitrogen permeameter. The obtained petrophysical parameters allows the identification of different hydraulic flow units (HFUs) and reservoir rock types

Gas pathway

(RRTs) encountered in the studied Wakar sandstones. HFUs and RRTs were interpreted based on some calculated parameters including normalized porosity index (NPI), reservoir quality index (RQI), and flow zone indicator (FZI) as well as the pore throat radius ( $R_{35}$ ) (Kolodzie, 1980; Amaefule et al., 1993):

Gas pathway

$$RQI = 0.0314\sqrt{K/\Phi} \tag{1}$$

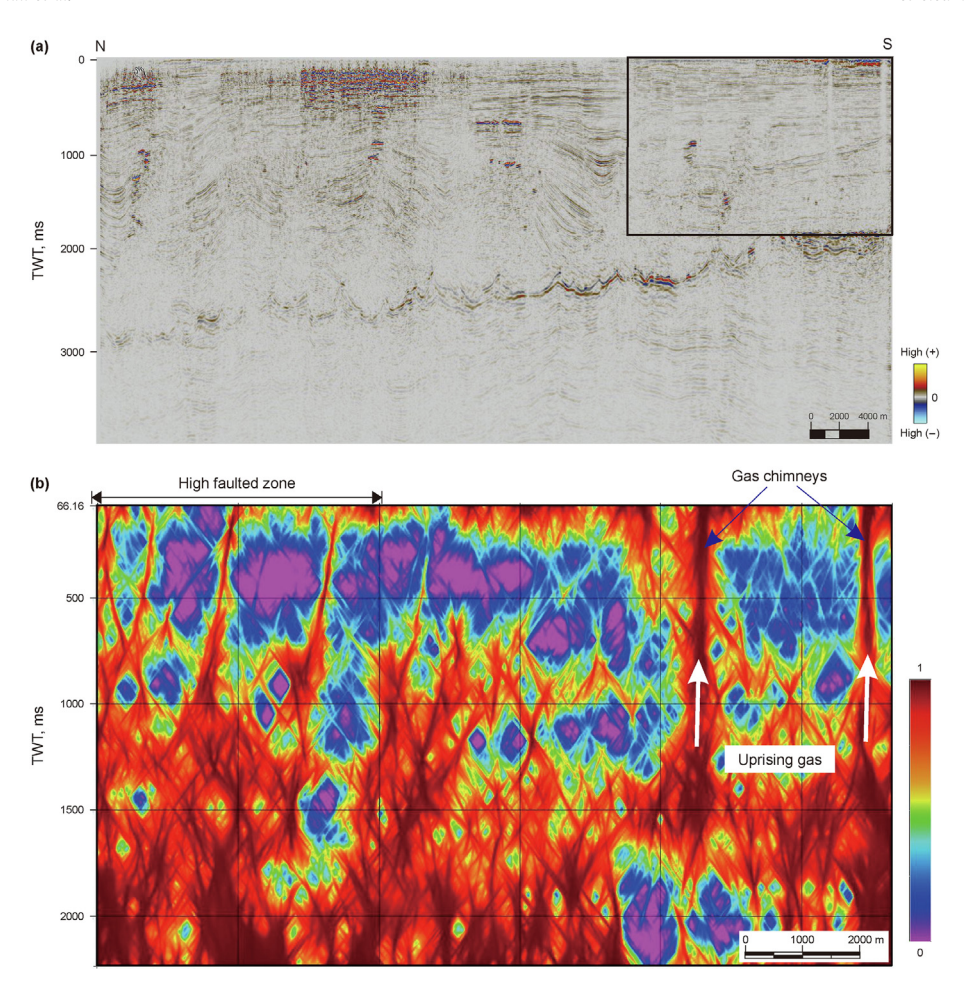


Fig. 6. (a) The original amplitude seismic section illustrating some vertical discrepancies interpreted as gas seepage regions (see the black rectangle); (b) A zoom on the rectangle in (a), after the fault likelihood (FL) attribute extraction highlights the poor data zones (chimneys) and the high fault zones that have maximum values (dark red and black colors) while the extended horizons and high amplitude zones have the minimum values (blue and pink colors).

$$NPI = \frac{\Phi}{1 - \Phi} \tag{2}$$

$$FZI = \frac{RQI}{NPI} \tag{3}$$

$$R_{35} = 5.395 \frac{K^{0.588}}{\Phi^{0.824}} \tag{4}$$

The coefficient of variation (*CV*) was calculated for all the petrophysical parameters to determine the extent of petrophysical heterogeneity (Yasser et al., 2022) as follows:

$$CV = \frac{\sigma}{\mu} \tag{5}$$

where  $\sigma$  is the standard deviation and  $\mu$  is the mean.

#### 4. Results and interpretations

#### 4.1. Seismic interpretation and gas seepage zones

The conventional phase of seismic data interpretation proceeded with the identification of key stratigraphic horizons (Figs. 3 and 4). The hydrocarbon-bearing Wakar Formation is bounded by

two seismic-stratigraphic boundaries separating the Wakar facies from the underlying Sidi Salem and overlying Rosetta formations, respectively. The base Rosetta is highly-erosive documenting the Messinian salinity crisis event and the onset of salt deposition in the circum-Mediterranean (Lofi et al., 2011a, 2011b; Leila and Moscariello, 2018, 2019). Wakar seismic facies consists of semitransparent, low to medium amplitude reflections. The seismic amplitude and continuity decreases basinwards where the seismic facies becomes more chaotic. Variation in seismic response suggests a lateral change in depositional facies. Notably, basin-fill seismic facies and amalgamated channels were observed in the vicinity of the studied wells (Figs. 3 and 4). Correlation with sedimentary cores reveals upward facies changes from coarse-grained cross-stratified sandstones and slumped sandstones into parallel laminated mudstones/siltstones. These facies are interpreted as turbiditic channel/levee complex facies. This is consistent with the fining-upward sedimentary succession where the cross-stratified sandstones represent the sediments of high-energy traction currents. Laminated mudstone facies at the top of the succession reflects an upward transition from traction to suspension deposition in agreement with the upward decrease in the turbiditic flow energy (e.g. Lowe, 1982; Kneller et al., 1997). The channel/levee complex deposits change laterally into hemiplegic and background mudstone facies.

Several gas pipes have been identified with some associated

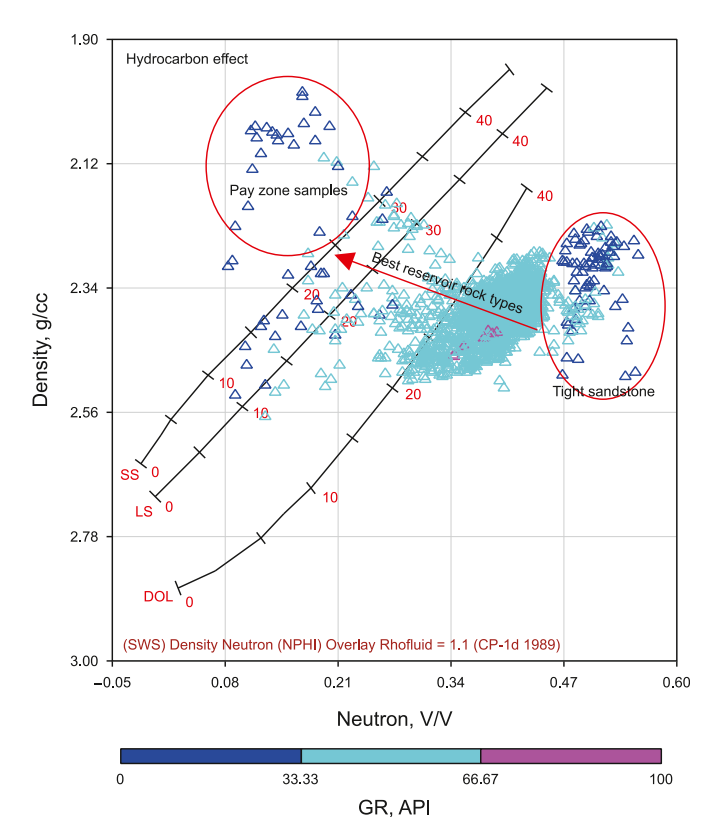


**Fig. 7.** Bulk density (*RHOB*) versus neutron porosity (*NPHI*) cross-plot demonstrates the matrix composition of the studied Wakar sediments.

features, such as pockmarks, bright anomalies, seepage out from seafloor, and BSRs (Figs. 3 and 4). Consequently, root-mean square "RMS" and sweetness attributes highlight occurrence of bright anomalies, heightened reflectors, and BSR with maximum amplitudes and faults and chimneys with the minimum amplitude range (Fig. 5). In addition, fault likelihood (FL) attribute shows gas chimneys appear as vertical plumes (Fig. 6). The gas plumes are associated with micro-faults that are rooting-down to the Rosetta salt (Figs. 3–6) typifying sub-salt gas generation and seepage. The gas-macro-seepages through gas chimneys appear as straight or slanted plumes where the gas rises toward the seabed via chimneys and along faulted zones after accumulating and migrating with high pressure out of the "kitchen" likely in the pre-Messinian rock units (Figs. 4–6).

# 4.2. Wireline logging interpretation

Interpretation of wireline logs allows identification of lithosaturation characteristics of the hydrocarbon bearing horizons. The density-neutron cross-plot demonstrates that Wakar Formation constitutes variable lithofacies types (Fig. 7). Notably, most silt-and mud-rich intervals (gamma ray >35 API) display bulk density (*RHOB*) values greater than 2.5 g/cm³ typifying a pore system infilled with either irreducible water, clay matrix and/or cement. On the other hand, the sand-rich horizons with gamma ray values < 35 API display *RHOB* values either as low as 2 gm/cm³ or greater than 2.3 gm/cm³, thereby typifying occurrence of two different sandstone rock types with variable litho-saturation properties (Fig. 7).

Wakar Formation sediments display several coarsening-upward patterns where sand/mud ratio increases and the shale volume decreases. These patterns are also characterized by upward increase in permeability (Fig. 8). Two, clean, coarse-grained sandstone bodies are reported at the top of the coarsening-upward patterns (level S-1, S-2). These sandstone bodies display blockyshaped gamma ray motif with values less than 40 API (Fig. 8). They are characterized by anomalously-high resistivity values typifying the presence of movable hydrocarbons. The sandstone bodies have good effective porosity (average > 20%), low shale volume and water saturation values (average < 10%, 35.5%, respectively). These characteristics suggest that level S-1, S-2 sandstone bodies consist of rock types differ from the underlying and overlying sediments.

Effective porosity versus water saturation (Buckles plot; Buckles, 1965) typifies a wide variation in the bound volume of water "BVW" values in the studied Wakar sediments (Fig. 9). Notably, low BVW values are associated with the clean sandstone bodies of levels S-1, S-2, whereas elevated BVW occur in clay-rich facies. These characteristics demonstrate the paramount impact of sedimentological characteristics and distribution of reservoir rock types on hydrocarbon accumulation and entrapment.

#### 4.3. Pore system characteristics

The studied cored intervals of Wakar Formation display wide ranges of porosity and permeability values. Helium porosity varies between 4.72% and 30.76% (average = 18.3%), whereas horizontal and vertical permeability values display average values of 61.8 milli-darcy (md) and 64.7 md, respectively. The CV value for porosity is 0.58, whereas those for horizontal and vertical permeability are 1.57 and 1.43, respectively. These values reflect a largescale permeability heterogeneity. On the horizontal versus vertical permeability cross-plot, most of the studied samples are plotted on the isotropic permeability line (Fig. 10(a)). On the other hand, the helium porosity versus horizontal and vertical permeability cross-plots reflect a wide heterogeneity in the pore system of the Wakar sandstones (Fig. 10(b) and (c)). Notably, sediments with porosity values > 10% display permeabilities 10 to 100-fold greater. Additionally, cores with permeability values > 100 md demonstrate a unique porosity-permeability trend where the latter decreases as porosity increases greater than 25%. We interpret that to the relative abundance of scattered dead-end pores which contribute porosity rather than permeability. Plotting horizontal permeability versus grain density elucidates that best permeable zones are those dominated by quartzose sandstones with grain densities in the range of 2.65–2.7 g/cm<sup>3</sup> (Schön, 1996, Fig. 10(d)). Thus, optimum reservoir quality in the region is restricted to the spatial distribution of the clean sandstone facies.

#### 4.4. Source rock characteristics

Elevated total organic carbon (TOC) values are observed in the Lower Miocene and Oligo-Miocene sediments of the Qantara and Tineh Formations (average = 1.15 w.t.% and 1.09 w.t.%, respectively), while those of other rock units display average TOC values < 1 w.t.% (Table 1). Rock-Eval  $S_1$  is less than 0.5 mg/g in all the studied samples. On the other hand, Rock-Eval  $S_2$  values are greater than  $S_1$ in all the studied samples, and the greatest  $S_2$  values are mostly associated with the Oligo-Miocene Tineh sediments (Table 1). Similarly, Rock-Eval S<sub>3</sub> values are greater in Qantara sediments than those in the other rock units. Measured values of Rock-Eval  $T_{\text{max}}$ increase progressively from the Pliocene Kafr El-Sheikh Formation (average = 408  $^{\circ}\text{C})$  to the Oligo-Miocene Tineh Formation (average = 436 °C). Average hydrogen index (HI) values > 100 mgHc/gTOC are only reported in the Wakar, Qantara and Tineh sediments. On the other hand, the average oxygen index (OI) values are greater in the Qantara and Tineh Formation than those in the

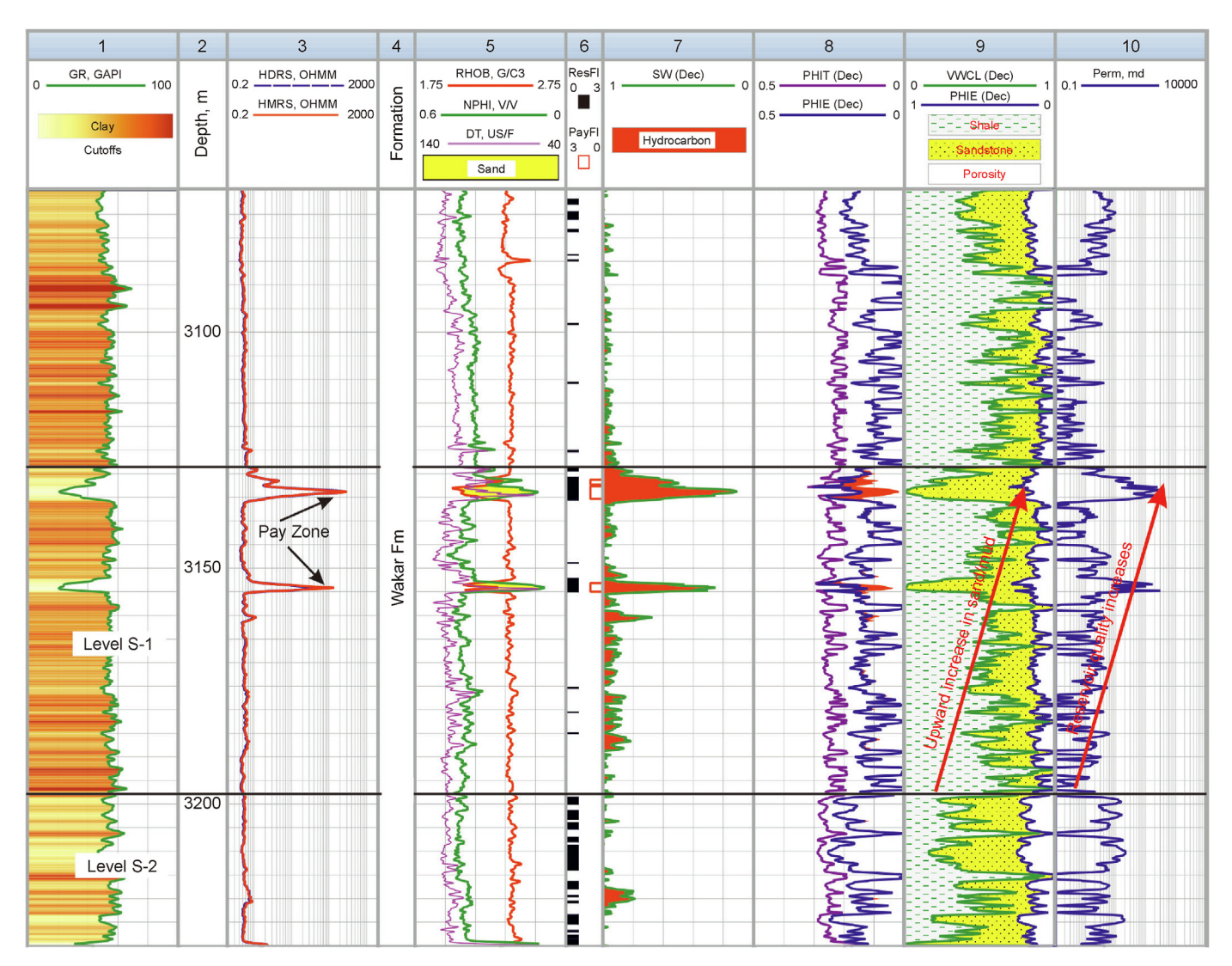


Fig. 8. Litho-saturation cross-plot of the Wakar formation, showing shale volume, total and effective porosities, water saturation in addition to pay and the reservoir zones of the PFM SE-1 well.

younger rock units. Average OI values  $< 100 \text{ mgCO}_2/\text{gTOC}$  are only observed in the Kafr El-Sheikh and Wakar sediments. The calculated values of production index (PI) are greater in the Kafr El-Sheikh and Wakar sediments than those in the Qantara and Tineh sediments. Average PI values greater than 0.1 are only observed in the Kafr El-Sheikh and Wakar sediments (Table 1). The measured vitrinite reflectance  $(\%R_0)$  displays a progressive increase with depth. Vitrinite reflectance values greater than 1 are only reported in Tineh Formation, while the average values in Kafr El-Sheikh and Wakar sediments are 0.46 and 0.58, respectively (Table 1).

# 4.5. Natural gas and condensate geochemistry

Molecular composition of the studied gases is dominated by CH<sub>4</sub> (>90%), with sub-ordinate contents of C<sub>2</sub> and C<sub>3</sub> components (average = 3.32% and 1.58%, respectively) (Table 2). Liquid hydrocarbon phases (C<sub>6+</sub>) occur in the range of 0.09% and 1.94%. Dryness coefficient (C<sub>1</sub>/( $\Sigma$ C<sub>1</sub>-C<sub>5</sub>)) ranges from 0.91 to 0.97. The gases display light  $\delta^{13}$ C<sub>1</sub> values < -49‰ and exhibit an isotopic pattern of  $\delta^{13}$ C<sub>1</sub> <  $\delta^{13}$ C<sub>2</sub> <  $\delta^{13}$ C<sub>3</sub> (Table 2). They have  $\delta$ DC<sub>1</sub> in the range of -163‰ and -191‰. The analyzed condensate sample shows a light API gravity (~48.8°) with abundant saturate fractions (>90%)

relative to aromatics and nitrogen, sulfur, oxygen "NSO"-compounds (Table 3). Saturates are represented mainly by light molecular weight n-alkanes ( $nC_5-nC_{15}$ ) (Fig. 11). Isoprenoids are common with elevated pristane/phytane "Pr/Ph" ratio of (>3), whereas isoprenoid/n-alkane ratios are less than 1 (Table 3). The  $\delta^{13}C_{\text{saturates}}$  and  $\delta^{13}C_{\text{aromatics}}$  are heavy < -30%, thus displaying a canonical variable (CV) value of -1.19. The  $C_7$ -hydrocarbon analysis demonstrates a relative abundance of dimethylpentane components (It) of 8.07, whereas the dimethylpentanes and dimethylcy-clopentane ratio (LnZ) value is -0.4 (Table 3).

# 5. Discussion

## 5.1. Reservoir rock-typing of the Wakar sandstones

Reservoir rock-typing (RRT) is an essential approach to improve the predictability of potential reservoir facies, thereby reducing the exploration risks (Masalmeh et al., 2012; Skalinski and Kenter, 2015; Tiab and Donaldson, 2015; Elmahdy et al., 2023). RRT encompasses a subdivision of the reservoir rocks into several distinctive units with geologically-controlled storage and flow properties (Guo et al., 2007; El Adl et al., 2021; Leila et al., 2022a,

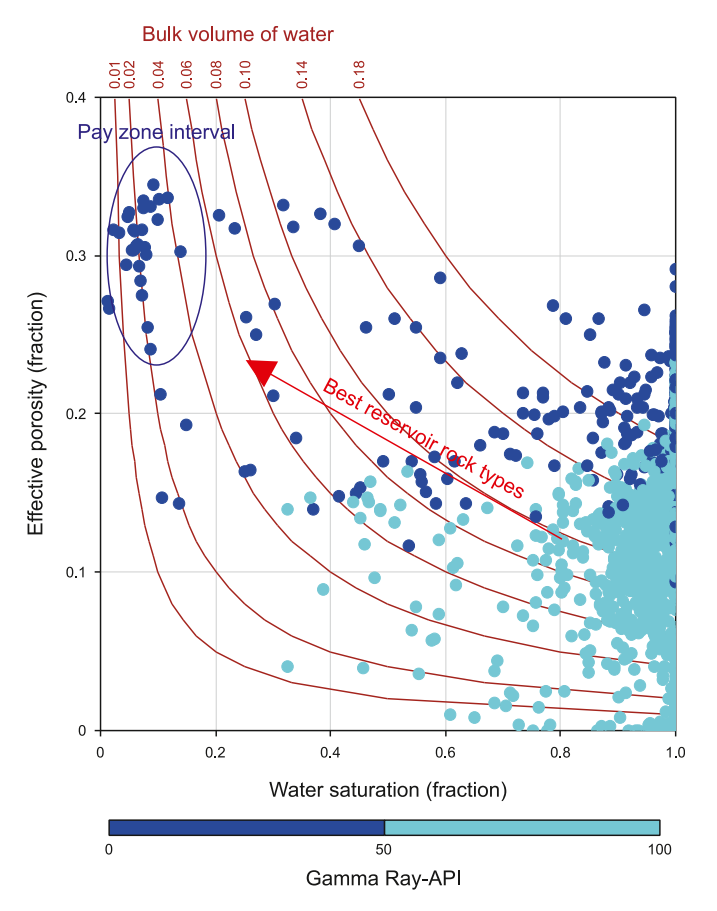


**Fig. 9.** Effective porosity versus water saturation (buckles plot) shows variations in bulk water volume in the sediments of Wakar formation in PFMSE-1 well.

2022b; Nabawy et al., 2023). Most of the Wakar sandstones display isotropic pore system (Fig. 10(a)), however, the degree of pore system connectivity vary greatly (Fig. 10(b) and (c)). Such variation in pore system connectivity despite its isotropism is likely controlled by lithofacies composition (Fig. 10(d)). Three reservoir rock-types (RRTI, RRTII, and RRTIII) with variable compositionallycontrolled pore system characteristics were interpreted (Table 4). RRTI sandstones have a pore system dominated by macropores and megapores ( $R_{35} > 10 \, \mu m$ ) with permeability values greater than 100 md (Fig. 12(a)). RRTI rocks constitute good hydraulic flow zones and are classified as hydraulic flow unit 4 (HFU4) (Fig. 12(b) and (c)). On the other hand, RRTII comprises those sediments with a slightlyheterogeneous pore system where micropores and mesopores are abundant, thus the permeability values are less than 100 md (Fig. 12(a)). RRTII facies have heterogeneous flow properties ranging from HFU1 to HFU3 (Fig. 12(c)). The poorest reservoir quality sediments are classified as RRTIII with a very tight pore system consists of disconnected micropores (Fig. 12(a)). RRTIII sediments have poor reservoir quality where the flow capacity is very low (Fig. 12(b) and (c)). Comparison between petrophysical reservoir quality (RQI), pore system ( $R_{35}$ ) and lithofacies reveals that the connected megapores of RRTI rocks are associated with high-energy turbidite channel facies dominated by massive and cross-stratified sandstones. While RRTII and RRTIII rocks are principally-associated with channel levees where the lithofacies change into laminated mud-rich sediments (Fig. 12(d)).

The vertical distribution of different RRTs displays a good correlation with sedimentary and seismic facies (Fig. 13). Notably, the poor reservoir quality RRTIII correlates with the low-amplitude, transparent seismic facies which corresponds to the mudstone and laminated mudstone facies. These facies either represent the hemiplegic background deposits. Lateral and vertical variation in seismic facies are associated with variation in RRTs where RRTII and RRTI rocks coincide with the prograding hummocky and basin-fill seismic facies. These facies correspond to the sandstone and silt-stone facies of a low-stand turbiditic wedge deposited offshore Nile Delta during the Early Messinian (Figs. 4 and 5; e.g. Dolson et al., 2005).

Reservoir rock-typing of the Upper Miocene reservoirs in the onshore Nile Delta revealed similar results where the depositional attributes enormously-influenced the petrophysical properties and distribution of the RRT (Leila and Moscariello, 2018, 2019; Leila, 2019; El Adl et al., 2021; Leila et al., 2021a). Notably, RRTI rocks of Wakar Formation are correlated with RRTII sediments of the deltaic onshore-equivalent Qawasim Formation (Leila and Moscariello, 2018, 2019). Thus, the Wakar sandstones have tighter pore system than that in the Qawasim Formation containing super-capillary pores with  $R_{35}$  values greater than 50  $\mu$ m despite their similar provenance (El-Sisi et al., 1996; Leila and Moscariello, 2018; Leila et al., 2023a, 2023b). Therefore, we hypothesize that deposition of the Wakar sandstones in relatively more distal conditions associated with a completely different diagenetic pathways resulting in more tightness for the pore system. Several authors have demonstrated that increasing marine influence allows pervasive eogenetic cementation with specific cements such as calcite and clays which block the intergranular pore spaces, thereby decreasing the pore system connectivity (Kim et al., 2007; Leila and Mohamed, 2020; El Adl et al., 2021).

#### 5.2. Hydrocarbon origin and source rock generation potential

Geochemical analyses on the studied rock units revealed a fair to good petroleum generation potential in some intervals, however, greater potentiality is observed in the Upper Miocene Wakar and Oligo-Miocene Tineh formations (Fig. 14(a)). These sediments have reached the thermal maturity level that allows a thermogenic generation of hydrocarbons (Fig. 14(b)). A certain level of thermal maturity is necessary for both clastic and non-clastic source rocks to promote kerogen cracking and thereby expulsion of hydrocarbons from the source rock to the reservoir (e.g. Ungerer et al., 1984; Peters and Cassa, 1994). The onset of thermogenic generation window has been reported as 0.6 %Ro which is equivalent to approximately 430 °C T<sub>max</sub> values (Peters, 1986; Tissot et al., 1987; Leila and Moscariello, 2017). At this maturity level, early mature liquid hydrocarbon phases will be produced. On the other hand, thermally-immature sediments can only generate biogenic dry gas (e.g. Bernard et al., 1978; Schoell, 1983; Whiticar, 1999; Leila et al., 2021b; Radwan et al., 2022b).

The most critical parameters that influence hydrocarbon generation from the source rocks are the type of the organic matter (kerogen type) and the degree of thermal maturation (Espitalié et al., 1985; Bordevave et al., 1993; Peters and Cassa, 1994). Hydrogen index (HI) versus Rock-Eval  $T_{\text{max}}$  cross-plot demonstrates that except the Pliocene sediments with pure type III kerogen, all the other rock units are enriched in type II kerogen with ability to generate mixed liquid and gas thermogenic hydrocarbons (Fig. 15(a)). Moreover, only Tineh sediments and some levels in the Wakar have reached the minimum thermal maturation required for generation of thermogenic hydrocarbon phases. Therefore, thermogenic hydrocarbons in the study region is exclusively-associated with the Wakar and Tineh organofacies (Fig. 15(b)). This is further supported by vitrinite reflectance results which demonstrated the capability of the Tineh organofacies to generate wet gas, whereas the Wakar and Kafr El-Sheikh facies are only able to produce

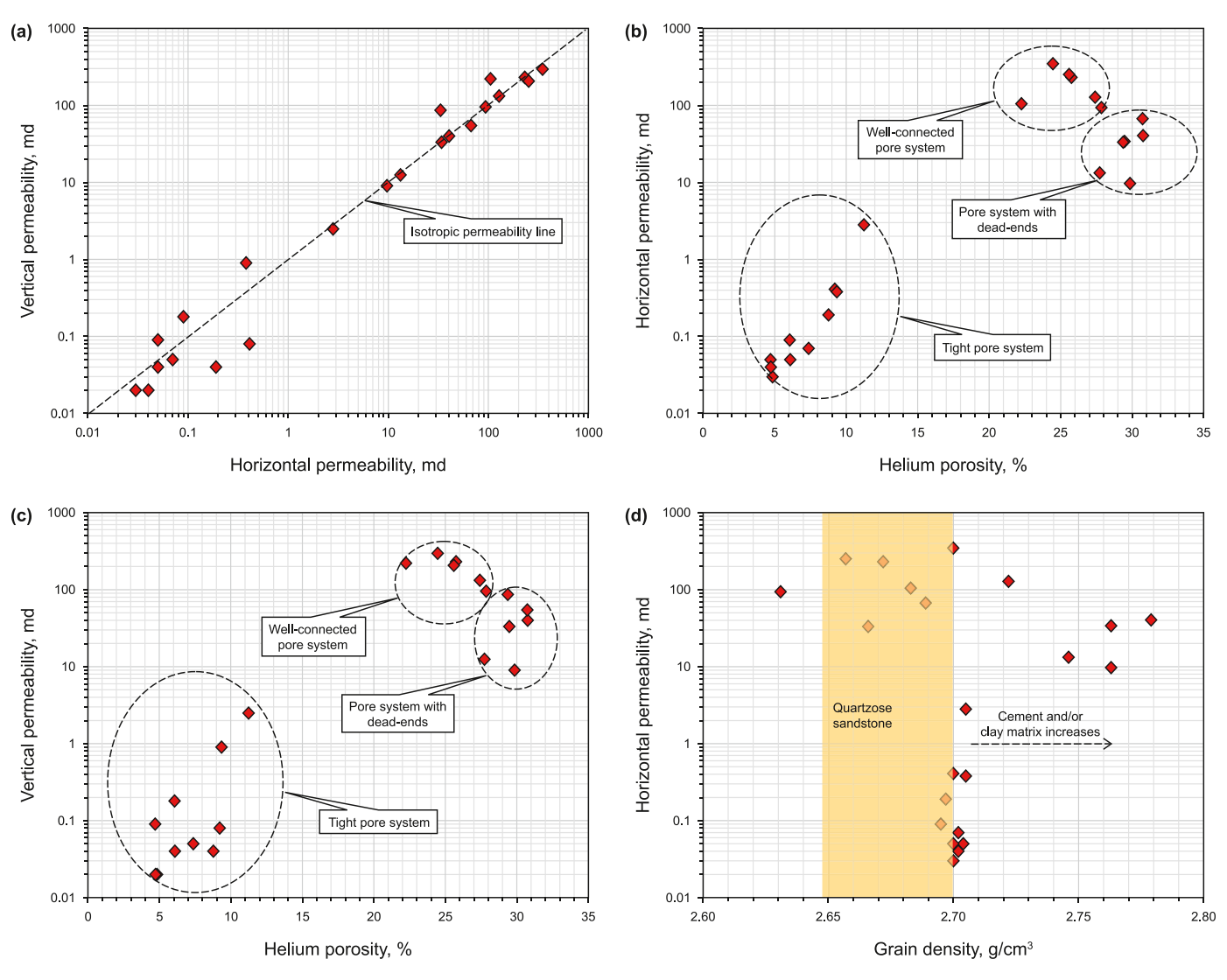


Fig. 10. Petrophysical cross-plots demonstrating the pore system characteristics of the studied cored interval in Wakar Formation sandstones.

immature oil or biogenic dry gas (Fig. 16).

Wet hydrocarbon gases often contains C<sub>2+</sub> hydrocarbons greater than 1% with dryness coefficient values less than 0.99 (Hunt, 1996; Whiticar, 1999). The studied gases contain  $C_{2+}$  hydrocarbons in the range of 2.5%-10% and display dryness coefficient values between 0.91 and 0.97, thereby confirming their wet gas composition. Wet gases usually have a thermogenic origin such as primary and secondary cracking of kerogen and pre-existing oil, respectively (Mackenzie and Quigley, 1988; Whiticar, 1999; Prenzhofer and Battani, 2003). However, the reported wide range of C<sub>2+</sub> hydrocarbon contents may point to gas generation via mixed processes. Observed isotopic patterns of  $C_1-C_3$  hydrocarbons displaying segmented curves are similar to mixed thermogenic-biogenic gases (Chung et al., 1988, Fig. 17a). Comparing molecular and isotopic composition of the studied gases with those reported in the Pliocene and Miocene reservoirs, offshore Nile Delta (Vandré et al., 2007) highlights a compositional similarity with the mixed thermogenic-biogenic Pliocene gases (Fig. 17(b)). Furthermore, the investigated gas samples display a large offset between  $\delta^{13}C_1$  and  $\delta^{13}C_2$  similar to those reported in the Pliocene gases of the Nile Delta, thus typifying their mixed origin where both biogenic and thermogenic processes contribute equally in the gas generation (Wu et al., 2016).

Molecular versus isotopic composition of light hydrocarbons  $(C_1-C_3)$  in cross-plots allows discrimination between variable genetic mechanisms (Bernard et al., 1978; Schoell, 1983; Prinzhofer and Battani, 2003; Milkov and Etiope, 2018; Leila et al., 2021b, 2022a, b). Molecular versus isotopic composition of the studied gas samples elucidates their thermogenic origin with a probable mixing with biogenic gases (Fig. 18(a)). Moreover, on cross-plot of carbon versus deuterium isotopic composition of methane, the studied gases are clustered in the field of oil-associated gas and overlap with those samples affected by secondary microbial processes (Fig. 18(b)). Noteworthy, values of  $\delta^{13}$ C in the  $C_1-C_3$  gas phases are often sensitive to thermal maturity level (Faber et al., 2015). Gases associated with early mature oils ( $\sim 0.6\%R_0$ ) display  $\delta^{13}C_1$  as light as -48% with  $\delta^{13}C_2$ ,  $\delta^{13}C_3$  of  $\sim -40\%$  and -36%, respectively. On the other hand, those generated at maturity levels close to  $1\%R_0$  have  $\delta^{13}C_1$  of -42.5 and  $\delta^{13}C_2$ ,  $\delta^{13}C_3$  of  $\sim -40\%$ and -36%, respectively. With increasing maturity ( $\sim 1.5\% R_0$ ), the  $\delta^{13}C_2$ ,  $\delta^{13}C_3$  get heavier as low as -28% and -27%. Based on that, the measured isotopic values for the studied gases reveal their generation at a maturity level greater than  $1\%R_0$  and less than 1.5% $R_0$ , however, the light values of  $\delta^{13}C_1$  as well as the wide offset between  $\delta^{13}C_1$ ,  $\delta^{13}C_2$  and  $\delta^{13}C_3$  point to mixing with microbial gases. Comparing the deduced maturity level of the studied gases

Summary of the minimum (Min.), maximum (Max.) and average (Av.) values obtained total organic carbon (TOC) and Rock-Eval pyrolysis analyses in the studied rock units encountered in the PFM Field wells.

Formation	Depth, m TOC, w.t.%	TOC, v	v.t.%		S <sub>1</sub> , mg/g	8/8		S <sub>2</sub> , mg/g	8	-,	S <sub>3</sub> , mg/g	g/		T <sub>max</sub> , C°		<i>H</i>	HI, mgHC/gTOC	IC/gTO		Ol, mg	<i>OI</i> , mgCO <sub>2</sub> /g <i>TOC</i>		PI			Vitrinite reflectan	Vitrinite reflectance, %R <sub>o</sub>	ίR₀
		Min.	Min. Max. Av. Min. Max. Av.	Av.	Min.	Max.		Min.	Max.	Av.	Min.	Max.	Av.	Min. Max. Av. Min. Max. Av. Min. Max. Av.	ſax. ≠		Min. Max. Av.	1ax. t		Min.	Min. Max. Av.	.	Min. Max. Av.	Max.		Min. Max Av.	Max	Av.
<b>Kafr El-Sheikh</b> ( $n = 21$ ) 1300–2570 0.73 1.14 0.92 0.14 0.29 0.21	1300-2570	0.73	1.14	0.92	0.14	0.29		0.42 1.14 0.67	1.14	0.67	0.52	1.12	0.75	400 4	419 4	408 5	50 1	116 7	72	55 1	143 8	84 (	0.17 0	0.3	0.24 0.39	0.39	0.54	0.46
Wakar $(n=28)$	2640-3429 0.54 0.98 0.77 0.14 0.27	0.54	0.98	0.77	0.14	0.27		0.73	1.8	1.21	0.43 (	0.97	7 89.0	413 4	434 4	424 1	104 2	217 1	158 (	65 1	129 8	) 88	0.10 0	0.26	0.14	0.54	09.0	0.58
Qantara $(n=2)$	3520-3580 1.14 1.17 1.15 0.06	1.14	1.17	1.15	90.0	0.11	0.08	2.5	3.07	2.78	1.20	1.33	1.26	413 4	414 4	413.5 2	214 2	269 2	241.5	105 1	114 1	109.5 (	0.02 0	0.03	0.025	ı	1	ı
Tineh $(n=48)$	3580-4490 0.60 1.81 1.09 0.01 0.22 0.06	09.0	1.81	1.09	0.01	0.22		0.11	2.58	1.03 0.81	0.81	2.72	2.72 1.53 420		447 4	436 1	14 2	222 9	91.91	61 3	316 1	146.8 0.02		0.20	0.073 1.1 1.26	1:1	1.26	1.18

Note: TOC = total organic carbon.  $S_1$  = volatile hydrocarbon content (mg HC/g rock);  $S_2$  = remaining hydrocarbon generative potential (mg HC/g rock);  $S_3$  = carbon dioxide yield (mg CO<sub>2</sub>/g rock);  $T_{max}$  = temperature at maximum of  $S_2$  peak; HI = hydrogen index  $(S_2 \times 100/TOC)$  (mg HC/g TOC); OI = oxygen index  $(S_3 \times 100/TOC)$  (mg  $CO_2/g$  TOC); and PI = production index  $(S_1/(S_1 + S_2))$ . with the maturity of vitrinite reflectance values of the studied organofacies (Fig. 16) suggests gas generation from the Tineh organofacies.

The  $\delta^{13}_{\text{saturates, aromatics}}$  values in the studied condensate are comparable to those in oils and bitumens produced by thermogenic cracking of mixed type II/III kerogen (Fig. 19(a)). This is further supported by the negative value of canonical variable (*CV*) as well as the relatively elevated Pr/Ph > 3 which point to a mixing marine and terrestrial input (Fig. 19(b); Sofer, 1984). Comparing the condensate sample with other liquid hydrocarbon families in and outside the Nile Delta (Zein El Din et al., 1990; Leila and Moscariello, 2017) elucidates a negative compositional correlation, thereby pointing to the generation of Wakar condensate from a different source rock. The mixed marine and terrestrial input in Wakar condensate is demonstrated by isoprenoid/n-alkane ratios ( $Pr/nC_{17}$  and  $Ph/nC_{18}$ ) highlighting its generation from a source rock containing mixed kerogen and deposited in sub-oxic depositional environment (Fig. 20; Shanmugam, 1985; Peters et al., 2005).

Geochemical characteristics of the studied condensate elucidate its generation from a type II kerogen which contain mixed marine and terrestrial organic materials. The wide difference between Wakar condensate and other Nile Delta oil samples highlights its unique hydrocarbon generation system. In the onshore Nile Delta, the Upper Cretaceous-Lower Paleogene organofacies were reported as the main source for light oil and condensate (Sharaf, 2003; Leila and Moscariello, 2017). Based on the present geochemical results. we hypothesize that the Wakar condensate could either be formed via secondary cracking of oil or have been generated from a less mature source rock than those reported for onshore hydrocarbons. This hypothesis is supported by the light  $nC_7$  results which confirms expulsion of the Wakar condensate at a relatively lower level of thermal maturity in comparison with those reported for onshore Nile Delta oils (Fig. 21). The expulsion maturity level of the Wakar condensate ( $\sim$ 0.85 % $R_0$ ) reveals its generation from a source rock at the peak oil window maturity probably from the Tineh organofacies when they entered the late oil-window maturity.

### 5.3. Implications for hydrocarbon exploration offshore Nile delta

Hydrocarbon exploration endeavors in the offshore Nile Delta are mostly focused on the biogenic gas plays either in the Pliocene turbidities (e.g. Scarab, Saffron, Sapphire etc.) or older clastic and non-clastic reservoirs (e.g. Zohr, Temsah) (Esestime et al., 2016; Mokhtar et al., 2016; Nabawy et al., 2018). Additionally, several gas escape features have been reported in the offshore Nile Delta and point to the presence of failed system, where either the reservoir or the seal did not exist (Ismail et al., 2021). Integration between seismic, wireline log, core analysis as well as geochemical results allows a better understanding for the petroleum system in PFDM Field, eastern offshore Nile Delta (Fig. 22(a)), Seismic profiles highlighted several small-scale disturbances in the seismic reflections resembling those described as gas chimneys, thereby reflecting fluid migration paths out of the pre-Messinian units' "kitchen" across the Miocene-Pliocene sequences to the seabed (Figs. 3 and 4; Dupré et al., 2007; Cathles et al., 2010; Rogers, 2015; Roy et al., 2016; Ismail et al., 2021).

Geochemical analyses reveal occurrence of mature organofacies in the Oligo-Miocene Tineh Formation. The maturity level of Tineh organofacies ( $\sim$ 1.2 % $R_{\rm o}$ ) suggests their ability to the wet gas phases accumulated in Wakar sandstone reservoirs. According to the paleogeographic reconstruction of northern Egypt during Late Oligocene (Fig. 22b; Dolson et al., 2014), deep marine deposition took place and incised canyons delivering clastics from the Gulf of Suez rift shoulders into the deep water caused accumulation of mixed marine and terrigenous facies. This agrees with our

**Table 2**Molecular and isotopic composition of the gas samples retrieved from the Wakar sandstones in PFM Field wells.

Well	Depth, m	C <sub>1</sub> , %	C <sub>2</sub> , %	C <sub>3</sub> , %	IC <sub>4</sub> , %	C <sub>4</sub> , %	IC <sub>5</sub> , %	C <sub>5</sub> , %	C <sub>6+</sub> , %	$\delta^{13}C_1$	$\delta^{13}C_2$	$\delta^{13}C_3$	$\delta DC_1$	Dryness coefficient
PFMSE-1	3130-3155	97.72	2.57	1.33	0.40	0.48	0	0.56	1.94	-56.1	-30.0	-29.0	-191	0.95
PFMD-2R	3775-3790	90.07	5.33	2.98	0.82	0.46	0.15	0.05	0.09	-49.4	-30.8	-30.3	-176	0.91
PFMD-2R	4340-4370	97.09	2.083121	0.428	0.10	0.06	0.06	0.04	0.12	-50.5	-31.0	-32.8	-163	0.97

Note: Dryness coefficient =  $C_1/(\Sigma C_1 - C_5)$ .

**Table 3**Bulk geochemical composition and biomarker ratios of the condensate retrieved from the Wakar sandstones in PFM Field wells.

Compositional attributes	Content
API	48.8
Saturates	95.6
Aromatics	3.7
Resin + NSO-compounds	0.7
δ <sup>13</sup> C <sub>Saturates</sub>	-28
$\delta^{13}C_{Aromatics}$	-27.2
Canonical variable (CV)	-1.194
Pr/Ph	3.49
Pr/nC <sub>17</sub>	0.97
Ph/nC <sub>18</sub>	0.27
Dimethylpentane components (It)	8.07
Dimethylpentanes and dimethylcyclopentane ratio ( <i>LnZ</i> )	-0.4

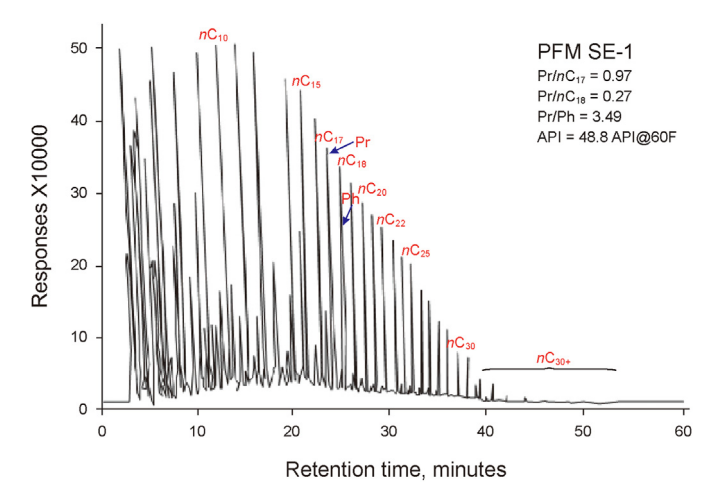


Fig. 11. Gas chromatogram illustrates the n-alkane distribution of the studied condensate.

geochemical results which confirmed enrichment of kerogen type II/III in the Tineh organofacies. Indeed, the biomarker signatures within the studied condensate confirm its generation from a mixed

marine/terrestrial organic matter. We hypothesize based in interpreted maturity level that that expulsion of condensate preceded gas generation and expulsion. Deep-seated faults cutting the subsalt successions act as the migration paths for generated condensate and gases from Tineh organo-facies to Wakar sandstone reservoirs (Fig. 22).

Wireline logging and core analysis revealed preferential accumulation of the expulsed hydrocarbon phases within the highenergy turbiditic channel facies which host clean quartzose sandstones dominated by macropores and megapores (RRTI). The sandstone pay zones (level S1, S2) correlate with the spatial distribution of RRTI rocks. Upward change into levee facies, the RRTI sandstones change into RRTII, RRTIII rocks which have poor hydraulic flow properties acting as baffle and barrier zones. Thus, hydrocarbon accumulation in the region is controlled by the spatial distribution of turbidite high-energy channel facies. Paleogeographic map of northern Egypt during Late Miocene before the MSC typifies deltaic deposition in the onshore (Qawasim Formation) and deep-water sedimentation offshore (Wakar Formation) (Fig. 22(c); Dolson et al., 2014). Lateral change in turbidite facies control the distribution of the reservoir rock types and hence the accumulation or seepage of hydrocarbons in the sub-salt successions, offshore Nile Delta.

#### 6. Conclusion

- Wet gas/condensate blend in the sub-salt Upper Miocene Wakar sandstones displays isotopic and molecular compositions reflect its thermogenic origin with signs of secondary microbial influence.
- Pliocene shales overlying the sandstone reservoirs are thermally-immature to generate thermogenic hydrocarbons, but likely contribute to microbial gas input.
- Organofacies with capability to generate wet gas and condensate are restricted to the sub-salt Oligo-Miocene Tineh sediments which display maturity levels up to 1.2 %R<sub>o</sub>.
- The geochemical characteristics of the studied gas/condensate blend demonstrate its generation from the sub-salt Tineh organofacies at different maturity levels. Gas expulsion took place at maturity level of ~1 %R<sub>o</sub>, while the expulsion maturity of condensate 0.85 %R<sub>o</sub>, thereby confirming accumulation of gas/

Petrophysical cutoff parameters of the reservoir rock types (RRT) reported in the Wakar sandstones in PFM Field wells.

Petrophysical Characteristics	RRTI	RRTII	RRTIII
Horizontal permeability, md	>200	>2.5	<1
Vertical permeability, md	>200	>2.0	<1
Helium porosity, %	>20	>20	<10
Permeability anisotropy	0.9-1.00	0.3-1.2	0.5-5
Grain density, g/cm <sup>3</sup>	2.65-2.70	2.63-2.77	2.69-2.74
RQI, μm	0.93-1.18	0.15-0.68	0.02-0.06
FZI, μm	2.70-3.65	1.23-2.38	0.47-0.65
R <sub>35</sub> , μm	9.09-12.08	1.34-6.45	0.18-0.51

Note: Reservoir quality index (RQI), flow zone indicator (FZI), and pore throat radius (R35).

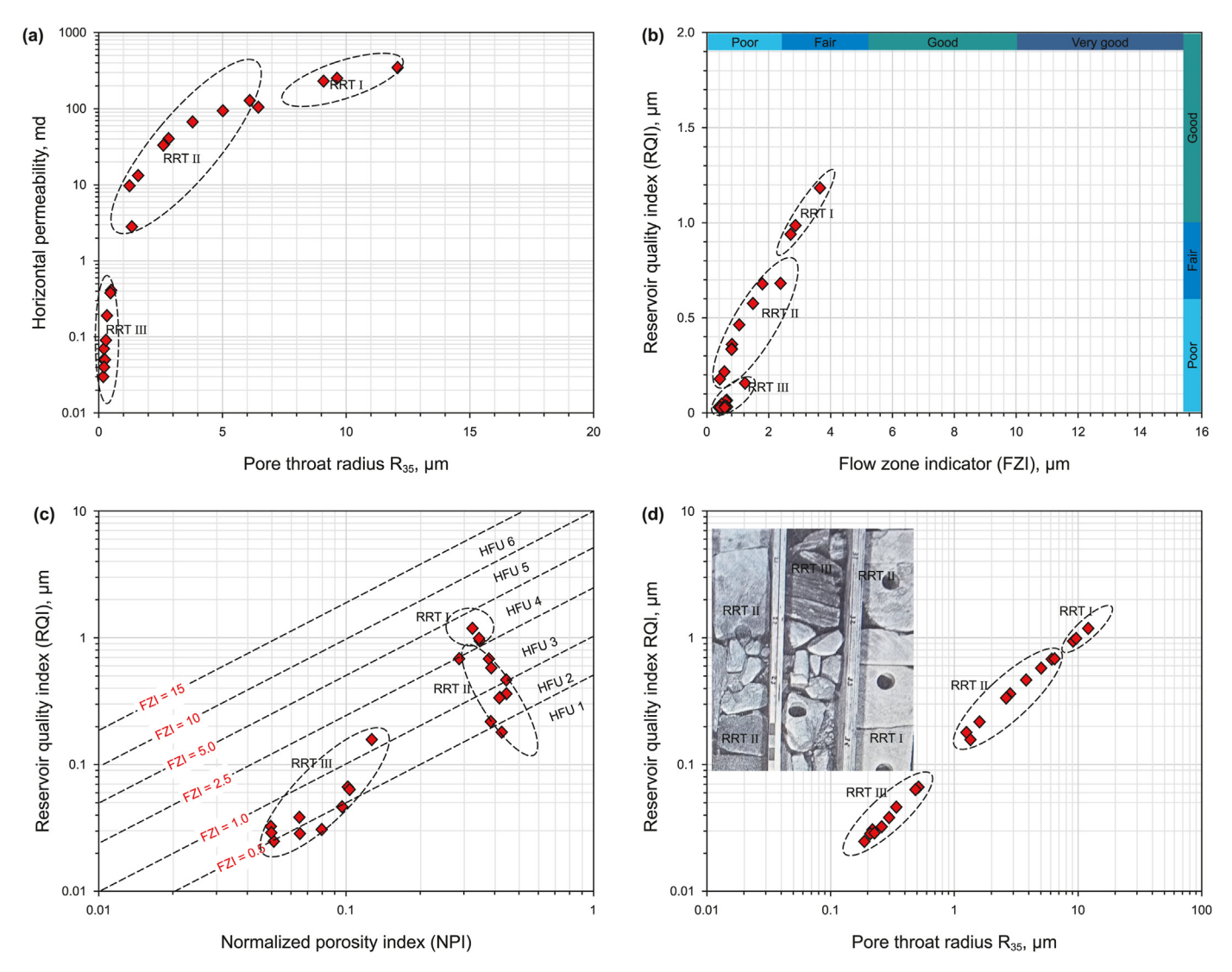


Fig. 12. Petrophysical reservoir rock-typing (RRT) of the studied cored interval of Wakar sandstones.

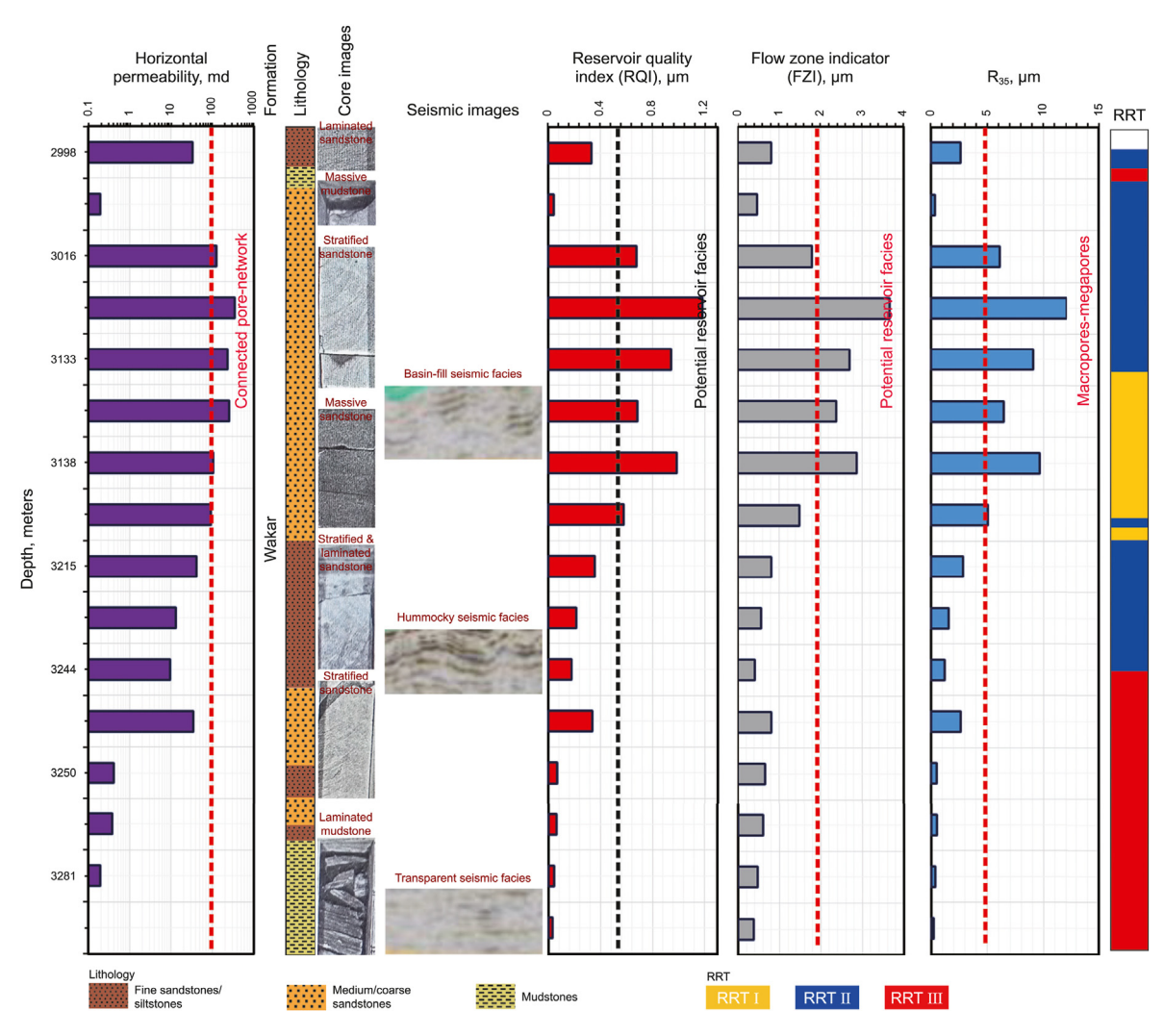


Fig. 13. Vertical distribution of different reservoir rock types (RRTs) encountered in the studied cored interval of Wakar Formation. The RRTs are correlated with corresponding sedimentary and seismic facies.

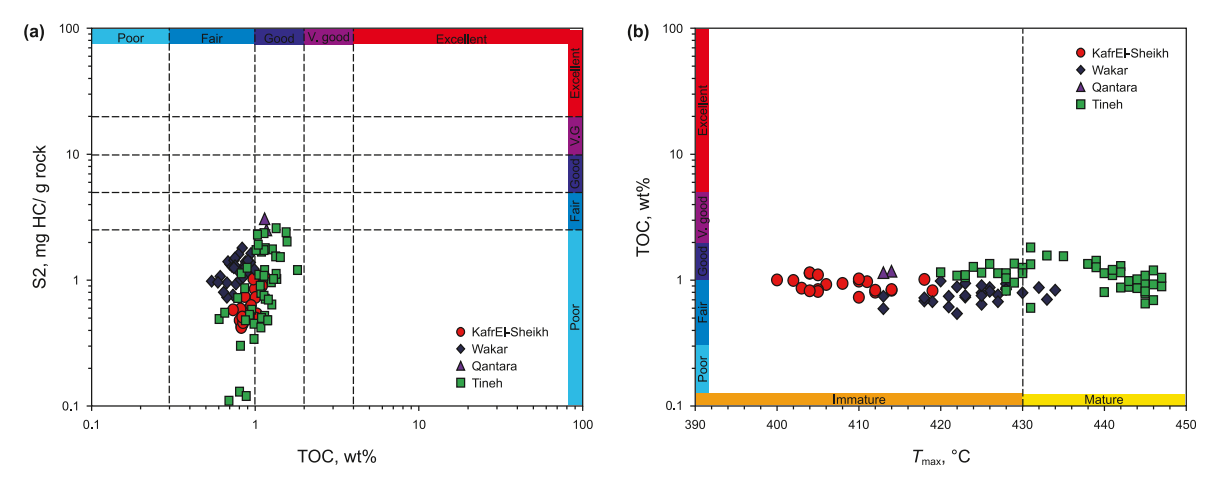


Fig. 14. Total organic carbon (TOC) versus Rock-Eval  $S_2$  and  $T_{max}$  cross-plots demonstrate the source rock potentiality of the studied rock units.

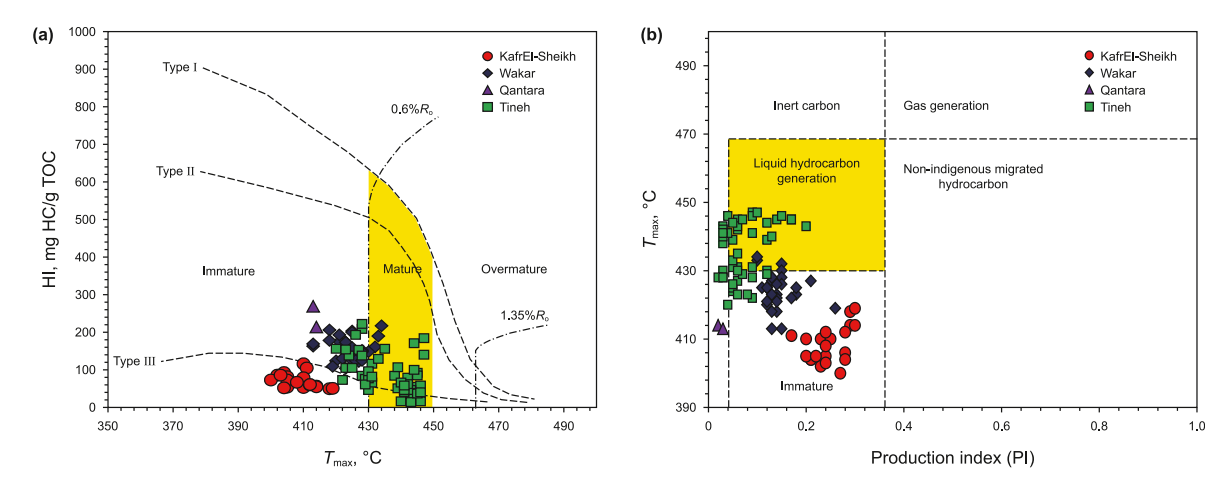
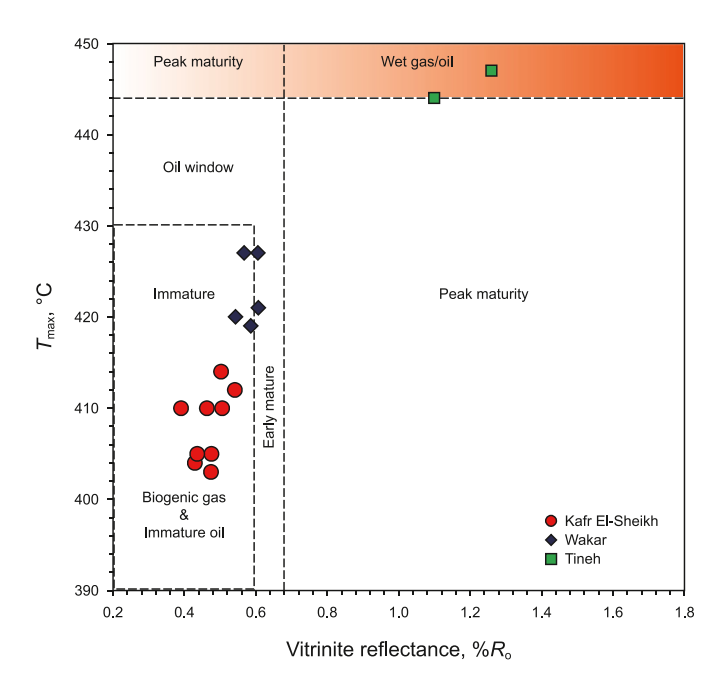


Fig. 15. Total organic carbon (TOC) versus Rock-Eval S2 and Tmax cross-plots demonstrate the source rock potentiality of the studied rock units.

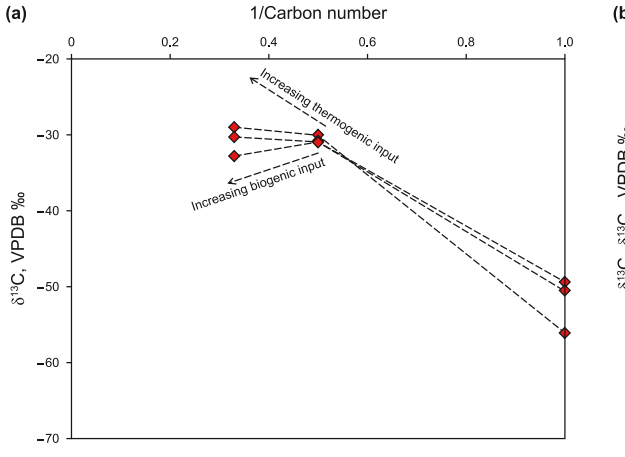


**Fig. 16.** Vitrinite reflectance ( $^{\otimes}R_{0}$ ) versus Rock-Eval  $T_{\max}$  cross-plot demonstrates the variation of thermal maturation level among the studied potential source rocks.

- condensate blend during the transition from late oil window to gas window maturities.
- Micro-faults and vertical disturbance in seismic reflections below and above the Messinian Rosetta salt provide evidence for gas seepage from the sub-salt organofacies.
- Gas seepage is reported where the hemiplegic facies exist. These
  facies consist mainly of low reservoir quality mudstone (RRTIII).
  On the other hand, hydrocarbon accumulation coincide with the
  turbidite channel/levee complex facies hosting good reservoir
  quality RRTI, RRTII sandstones.

#### **CRediT authorship contribution statement**

Mahmoud Leila: Writing — review & editing, Writing — original draft, Visualization, Validation, Software, Resources, Methodology, Investigation, Formal analysis, Data curation, Conceptualization. Ahmed A. Radwan: Writing — review & editing, Writing — original draft, Supervision, Resources, Project administration, Methodology, Investigation, Data curation, Conceptualization. Amir Ismail: Writing — review & editing, Writing — original draft, Visualization, Validation, Software, Resources, Project administration, Investigation, Formal analysis, Data curation, Conceptualization. Emad A. Eysa: Writing — review & editing, Writing — original draft, Visualization, Validation, Supervision, Software, Resources, Project administration, Formal analysis, Data curation.



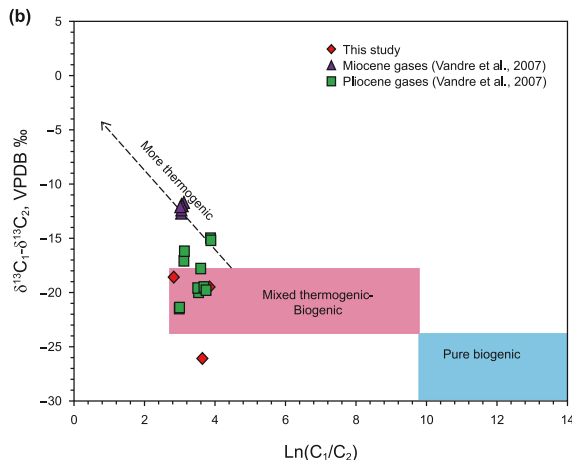
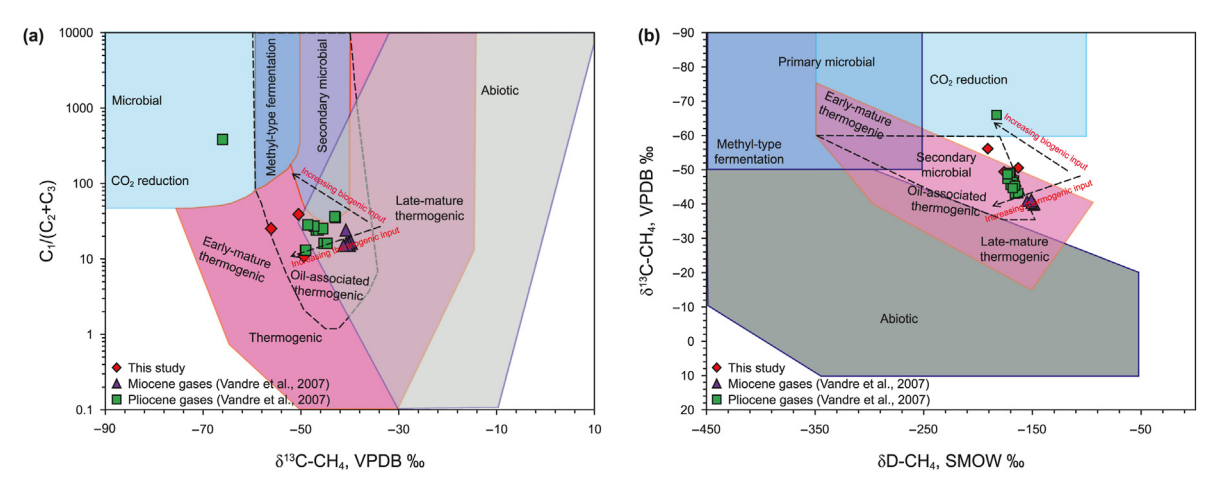


Fig. 17. Molecular versus isotopic composition cross-plots of the studied Wakar gases illustrate their mixed thermogenic-biogenic origin. Interpretation fields are from Wu et al. (2016).



**Fig. 18.** Genetic characteristics of the investigated Wakar gases based on integration between their molecular and isotopic composition following the interpretation fields of Milkov and Etiope (2018). Interpretation fields (CR – CO<sub>2</sub> reduction, SM – secondary microbial, F – methyl-type fermentation, OA – oil-associated thermogenic gas, EMT – early mature thermogenic gas, LMT – late mature thermogenic gas).

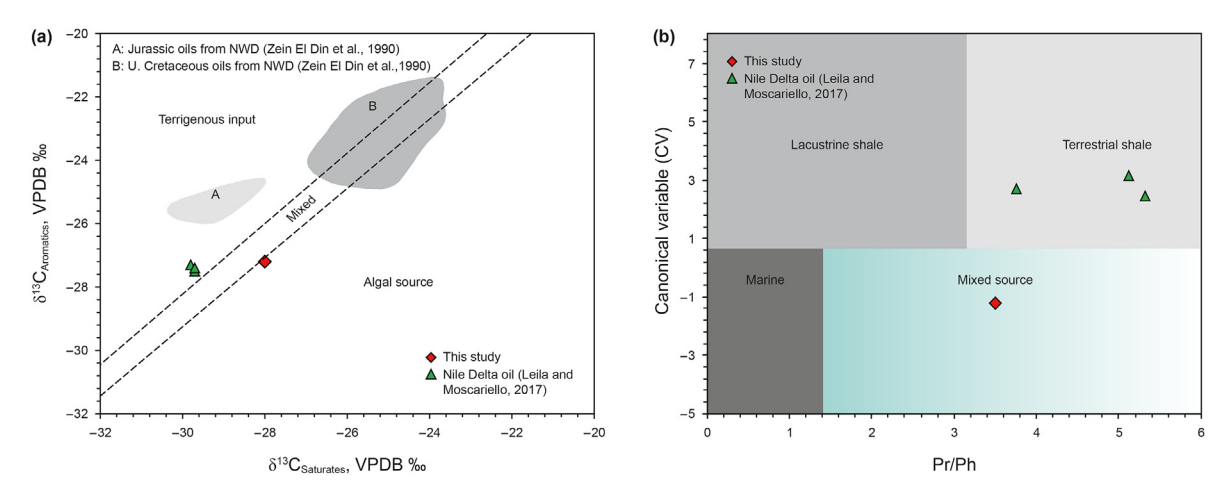
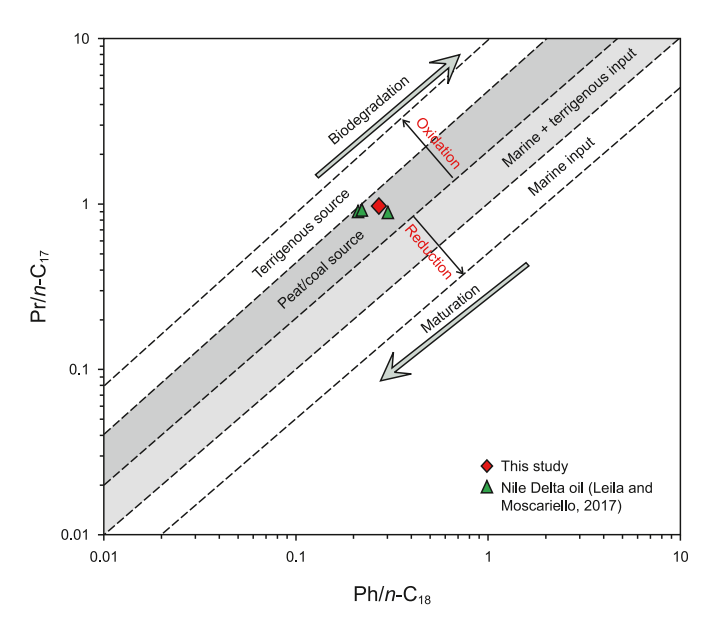
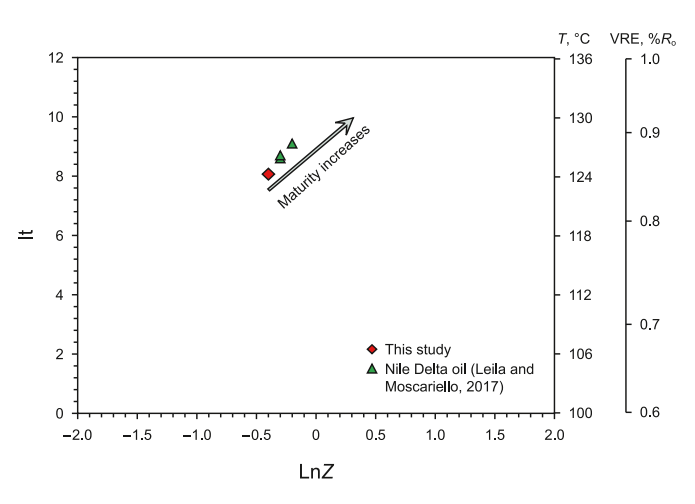


Fig. 19. Isotopic composition  $\delta^{13}C_{saturates}$  versus  $\delta^{13}C_{aromatics}$  demonstrates the mixed organic input in the Wakar condensate sample (a); isoprenoid ratio versus canonical variable (CV) confirms the mixed source of the investigated Wakar condensate (b).



**Fig. 20.** Isoprenoid/n-alkane ( $Pr/nC_{17}$  and  $Ph/nC_{18}$ ) cross-plot illustrates the t depositional environment of the Wakar condensate. Interpretation fields are after Shanmugam (1985).



**Fig. 21.**  $C_7$ -derived expulsion temperature and maturity deduced for the studied Wakar condensate sample based on natural log values for dimethylpentane ratio (It) and ethylpentane, dimethylpentane, and dimethylcyclopentane ratio (LnZ). Equivalent vitrinite reflectance values (VRE) were deduced based on the average geothermal gradient in the Nile Delta (Riad et al., 1989).

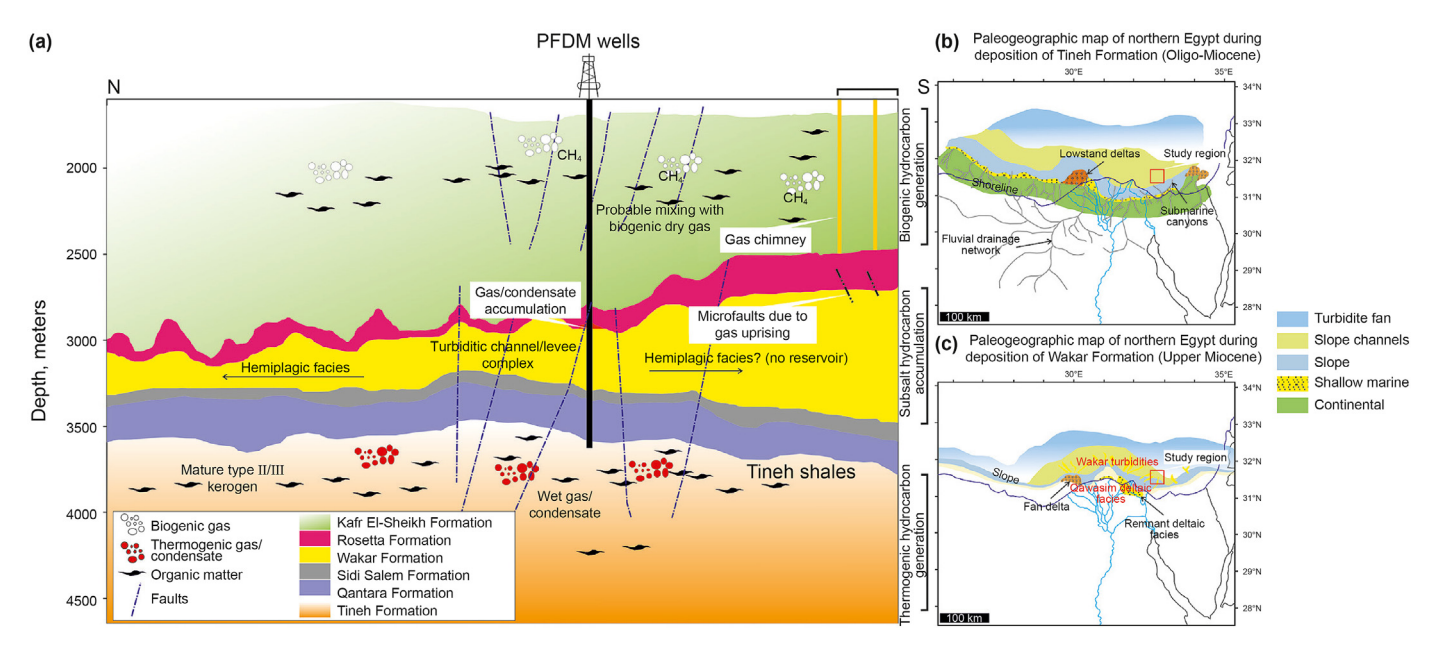


Fig. 22. An illustrative diagram (not to scale) demonstrates the elements of the sub-salt petroleum system in the eastern offshore part of the Nile Delta (a), paleogeographic maps illustrates the depositional setting of northern Egypt including the study region during Oligo-Miocene (b), and Late Miocene (c).

#### Declaration of interest

The authors want to declare that they do not have any conflict of interests to disclose.

#### Acknowledgement

The authors wish to express their gratitude to the Egyptian General Petroleum Corporation (EGPC) and PETROBEL Petroleum Company, Egypt, for granting the necessary raw data required for the completion of this study. Amir Ismail expresses his gratitude to the Fulbright Egypt Commission for awarding him a postdoctoral scholarship to Texas A&M University, Corpus Christi where he carried out a part of this study.

# References

Abdelwahhab, M.A., Radwan, A.A., Mahmoud, H., Mansour, A., 2022. Geophysical 3Dstatic reservoir and basin modeling of a Jurassic estuarine system (JG-Oilfield, Abu Gharadig basin, Egypt). J. Afr. Earth Sci. 225, 105067. https://doi.org/ 10.1016/i.jseaes.2021.105067.

Amaefule, J.O., Altunbay, M., Tiab, D., Kersey, D., Keelan, D., 1993. Enhanced reservoir description: using core and log data to identify hydraulic (flow) units and predict permeability in uncored intervals/wells. SPE Annual Technical Conference and Exhibition, Houston, October, pp. 205–220. https://doi.org/10.2118/ 26436-MS.

Asquith, G., Gibson, C., 1982. Basic Well Log Analysis for Geologists. AAPG, Tulsa Oklahoma USA, p. 216. https://doi.org/10.1306/Mth3425.

Behar, F., Beaumont, V., Penteado, H., 2001. Rock-Eval 6 technology: performances and developments. Oil Gas Sci. Technol. 56 (2), 111–134. https://doi.org/ 10.2516/ogst:2001013.

Bernard, B.B., Brooks, J.M., Sackett, W.M., 1978. Light hydrocarbons in recent Texas continental shelf and slope sediments. J. Geophys. Res.: Oceans 83 (C8), 4053–4061. https://doi.org/10.1029/JC083iC08p04053.

Bertello, F., Barsoum, K., Dalla, S., Guessarian, S., 1996. Temsah discovery: a giant gas field in a deep sea turbidite environment. 13th EGPC Exp. Prod. Conf. 1, 165—180. Cairo, Egypt.

Bordevave, M.L., Espitalie, J., Leplat, P., Oudin, J., Vandenbroucke, M., 1993. Screening techniques for source rock evaluation. In: Bordevave, M.L. (Ed.), Applied Petroleum Geochemistry. Paris Editions Technip, pp. 217–278. https://eurekamag. com/research/019/958/019958006.php.

Buckles, R.S., 1965. Correlating and averaging connate water saturation data. J. Can. Petrol. Technol. 9 (1), 42–52. https://doi.org/10.2118/65-01-07.

Cathles, L.M., Su, Z., Chen, D., 2010. The physics of gas chimney and pockmark formation, with implications for assessment of seafloor hazards and gas sequestration. Mar. Petrol. Geol. 27 (1), 82–91. https://doi.org/10.1016/

#### j.marpetgeo.2009.09.010.

Chung, H.M., Gormly, J.R., Squires, R.M., 1988. Origin of gaseous hydrocarbons in subsurface environments: theoretical considerations of carbon isotope distribution. Chem. Geol. 71 (1–3), 97–104. https://doi.org/10.1016/0009-2541(88) 90108-8

Clauzon, G., 1982. Le canyon Messinien du Rhone: une preuve decisive du 'dessicated deep-basin model' (Hsü, Cita and Ryan, 1973). Bull. Soc. Geol. Fr. 24, 231–246. https://doi.org/10.2113/GSSGFBULL.S7-XXIV.3.597.

Dewan, J.T., 1983. Essentials of Modern Open-Hole Log Interpretation. Pennwell Publications. Tulsa Oklahoma, p. 361.

Dolson, J.C., Atta, M., Blanchard, D., Sehim, A., Villinski, J., Loutit, T., Romine, K., 2014. Egypt's future petroleum resources: a revised look in the 21<sup>st</sup> Century. In: Marlow, L., Kendall, C., Yose, L. (Eds.), Petroleum Systems of the Tethyan Region, vol. 106. AAPG Mem, Tulsa, Oklahoma, pp. 143–178. https://doi.org/10.1306/13431856M106713.

Dolson, J.C., Boucher, P.J., Siok, J., Deppard, B., 2005. Key challenges to realizing full potential in an emerging giant gas province, Nile Delta/Mediterranean offshore, deep water, Egypt. In: Doré, A., Vining, B. (Eds.), Petroleum Geology, North-West Europe and Global Perspectives, Geological Society of London, Petroleum Geology Conference Series No. 6, Proc. 6<sup>th</sup> Petroleum Geology Conference, pp. 607–624. https://doi.org/10.1144/0060607.

Dupré, S., Woodside, J., Foucher, J.P., Lange, G., Mascle, J., Boetius, A., Mastalerz, V., Stadnitskaia, A., et al., 2007. Seafloor geological studies above active gas chimneys off Egypt (central nile deep sea fan). Deep Sea Res. Oceanogr. Res. Pap. 54 (7), 1146–1172. https://doi.org/10.1016/j.dsr.2007.03.007.

El Adl, H., Leila, M., Ahmed, M.A., Anan, T., El Shahat, A., 2021. Integrated sedimentological and petrophysical rock-typing of the messinian abu madi formation in south batra gas field, onshore nile delta, Egypt. Mar. Petrol. Geol. 124, 104835. https://doi.org/10.1016/j.marpetgeo.2020.104835.

Elmahdy, M., Radwan, A.A., Nabawy, B.S., Abdelmaksoud, A., Nastavkin, A., 2023. Integrated geophysical, petrophysical and petrographical characterization of the carbonate and clastic reservoirs of the Waihapa Field, Taranaki Basin, New Zealand. Mar. Petrol. Geol. 151, 106173. https://doi.org/10.1016/ j.marpetgeo.2023.106173.

El Matboly, E., Leila, M., Peters, K., El Diasty, W., 2022. Oil biomarker signature and hydrocarbon prospectivity of paleozoic versus mesozoic source rocks in the Faghur–Sallum basins, Egypt's Western Desert. J. Petrol. Sci. Eng. 217, 110872. https://doi.org/10.1016/j.petrol.2022.110872.

El-Sisi, Z., Sharaf, L., Yehia, H., Dawood, A., Hassouba, A., 1996. Source of Clastic Supply to the Sidi Salem and Abu Madi Reservoirs of the Nile Delta: a Province Study, vol. 1. Proc. 13<sup>th</sup> EGPC Exp. Prod. Conf., Cairo, Egypt, pp. 291–296.

Esestime, P., Hewitt, A., Hodgson, N., 2016. Zohr—A newborn carbonate play in the levantine basin, east-mediterranean. First Break 34 (2), 87–93. https://doi.org/10.3997/1365-2397.34.2.83912.

Espitalié, J., Deroo, G., Marquis, F., 1985. La pyrolyse Rock-Eval et ses applications. Deuxième partie. Rev. Inst. Fr. Petrol 40 (6), 755–784. https://doi.org/10.2516/ogst:1985045.

Fathy, D., Wagreich, M., Fathi, E., Ahmed, M., Leila, M., Sami, M., 2023. Maastrichtian anoxia and its influence on organic matter and trace metal patterns in the southern tethys realm of Egypt during greenhouse variability. ACS Omega 8 (22), 19603–19612. https://doi.org/10.1021/acsomega.3c01096.

Faber, E., Schmidt, M., Feyzullayev, A., 2015. Geochemical hydrocarbon exploration—insights from stable isotope models. Oil Gas Eur. Mag. 41, 93—98.

- Gammaldi, S., Ismail, A., Zollo, A., 2022. Fluid accumulation zone by seismic attributes and amplitude versus offset analysis at Solfatara volcano, Campi Flegrei, Italy. Front. Earth Sci. 10, 866534. https://doi.org/10.3389/feart.2022.866534.
- Guo, G., Diaz, M.A., Paz, F., Smalley, J., Waninger, E., 2007. Rock typing as an effective tool for permeability and water-saturation modelling: a case study in a clastic reservoir in the Oriente Basin. Res. Eval. & Eng. 10 (6), 730–739. https://doi.org/ 10.2118/97033-PA.
- Hassan, M., Leila, M., Ahmed, A., Issa, G., Hegab, O., 2023a. Geochemical characteristics of natural gases and source rocks in Obayied sub-basin, north Western Desert, Egypt: implications for gas-source correlation. Acta Geochim 42, 241–255. https://doi.org/10.1007/s11631-022-00576-5.
- Hassan, A., Radwan, A., Mahfouz, K., Leila, M., 2023b. Sedimentary facies analysis, seismic interpretation, and reservoir rock typing of the syn-rift Middle Jurassic reservoirs in Meleiha concession, north Western Desert, Egypt. J. Petrol. Expl. Prod. https://doi.org/10.1007/s13202-023-01677-4.
- Hsü, K.J., Cita, M.B., Ryan, W.B.F., 1973. The origin of the Mediterranean evaporites. In: Kaneps, A. (Ed.), Leg 13, vol. 13. Initial Reports of the Deep Sea Drilling Project, pp. 1203–1231. http://www.deepseadrilling.org/13/volume/dsdp13pt2\_43.pdf
- Hunt, J.M., 1996. Petroleum Geochemistry and Geology. W.H. Freeman and Company, New York, p. 332.
- Hussein, I., Abd-Allah, A., 2001. Tectonic evolution of the northeastern part of the African continental margin, Egypt. J. Afr. Earth Sci. 33, 49–69. https://doi.org/10.1016/S0899-5362/01/90090-9
- Hyndman, R.D., Spence, G.D., 1992. A seismic study of methane hydrate marine bottom simulating reflectors. J. Geophys. Res. 97, 6683–6698. https://doi.org/ 10.1029/92JB00234.
- Ismail, A., Ewida, H.F., Al-Ibiary, M.G., Gammaldi, S., Zollo, A., 2020. Identification of gas zones and chimneys using seismic attributes analysis at the Scarab field, offshore, Nile Delta, Egypt. Petrol. Res. 5 (1), 59–69. https://doi.org/10.1016/ j.ptlrs.2019.09.002.
- Ismail, A., Ewida, H.F., Al-Ibiary, M.G., Nazeri, S., Salama, N., Gammaldi, S., Zollo, A., 2021. The detection of deep seafloor pockmarks, gas chimneys, and associated features with seafloor seeps using seismic attributes in the West offshore Nile Delta, Egypt. Explor. Geophys. 52 (4), 388–408. https://doi.org/10.1080/08123985.2020.1827229.
- Ismail, A., Ewida, H.F., Nazeri, S., Al-Ibiary, M.G., Zollo, A., 2022. Gas channels and chimneys prediction using artificial neural networks and multi-seismic attributes, offshore West Nile Delta, Egypt. J. Petrol. Sci. Eng. 208, 109349. https:// doi.org/10.1016/j.petrol.2021.109349.
- Ismail, A., Radwan, A., Leila, M., Eysa, E., 2024. Integrating 3D subsurface imaging, seismic attributes, and wireline logging analyses: implications for a high resolution detection of deep-rooted gas escape features, eastern offshore Nile Delta, Egypt. J. Afr. Earth Sci. 213, 105230. https://doi.org/10.1016/j.jafrearsci.2024.105230.
- Kamel, H., Eita, T., Sarhan, M., 1998. Nile Delta Hydrocarbon Potentiality, Egypt, vol. 1. 14<sup>th</sup> EGPC Expl. Prod. Conf., Cairo, Egypt, pp. 485–503.
- Kim, J.C., Lee, Y.I., Hisada, K., 2007. Depositional and compositional controls on sandstone diagenesis, the Tetori group (Middle Jurassic-Early Cretaceous), central Japan. Sed. Geol. 195, 183–202. https://doi.org/10.1016/ j.sedgeo.2006.08.011.
- Kneller, B.C., Bennet, S.J., McCaffrey, W.D., 1997. Velocity and turbulence structure of gravity currents and internal solitary waves: potential sediment transport and the formation of wave ripples in deep waters. Sediment. Geol. 112, 235–250. https://doi.org/10.1016/S0037-0738(97)00031-6.
- Kolodzie, S., 1980. Analysis of pore throat size and use of the Waxman-Smits equation to determine OOIP in Spindle Field, Colorado. SPE Annual Technical Conference and Exhibition. SPE, Dallas, Texas, 9382-MS. https://doi.org/10.2118/ 9382-MS
- Lashin, A., Abd El Aal, M., 2005. Contribution of AVO and multi attribute analysis in delineating the fluid content and rock properties of the gas-bearing reservoirs in the Northeastern part of Nile Delta, Egypt. J. Appl. Geophys. 4 (2), 279—301. https://doi.org/10.1016/j.ejpe.2017.09.002.
- Leila, M., 2019. Clay minerals distribution in the pre-, syn-Messinian salinity crisis sediments of the onshore Nile Delta, Egypt: mineral origin and implications on the reservoir quality. J. Afr. Earth Sci. 154, 35–48. https://doi.org/10.1016/ i.iafrearsci.2019.03.016.
- Leila, M., Moscariello, A., 2017. Organic geochemistry of oil and natural gas in the West Dikirnis and El-Tamad fields, onshore Nile Delta, Egypt: interpretation of potential source rocks. J. Petrol. Geol. 40 (1), 37–58. https://doi.org/10.1111/ ips12663
- Leila, M., Moscariello, A., 2018. Depositional and petrophysical controls on the volumes of hydrocarbons trapped in the Messinian reservoirs, onshore Nile Delta, Egypt. Petrol. Times 4 (3), 250–267. https://doi.org/10.1016/ j.petlm.2018.04.003.
- Leila, M., Moscariello, A., 2019. Seismic stratigraphy and sedimentary facies analysis of the pre- and syn-Messinain salinity crisis sequences, onshore Nile Delta, Egypt, Implications for reservoir quality prediction. Mar. Petrol. Geol. 101, 303—321. https://doi.org/10.1016/j.marpetgeo.2018.12.003.
- Leila, M., Mohamed, A., 2020. Diagenesis and petrophysical characteristics of the shallow Pliocene sandstone reservoirs in the Shinfas gas field, onshore Nile delta, Egypt. J. Pet. Explor. Prod. Technol. 10, 1743—1761. https://doi.org/10.1007/ s13202-020-00873-w.

- Leila, M., Moscariello, A., Kora, M., Mohamed, A., Samankassou, E., 2020. Sedimentology and reservoir quality of a Messinian mixed siliciclastic carbonate succession, onshore Nile Delta, Egypt. Mar. Petrol. Geol. 112, 104076. https://doi.org/10.1016/j.marpetgeo.2019.104076.
- Leila, M., Ali, E., Abu El-Magd, A., Alwan, L., Elgendy, A., 2021a. Formation evaluation and reservoir characteristics of the Messinian Abu Madi sandstones in Faraskour gas field, onshore Nile delta, Egypt. J. Pet. Explor. Prod. Technol. 11, 133–155. https://doi.org/10.1007/s13202-020-01011-2.
- Leila, M., Levy, D., Battani, A., Piccardi, L., Segvic, B., Badurina, L., Pasquet, G., Cambaudon, V., Moretti, I., 2021b. Origin of continuous hydrogen flux in gas manifestations at the Larderello geothermal field, Central Italy. Chem. Geol. 585, 120564. https://doi.org/10.1016/j.chem.geo.2021.120564.
- Leila, M., Awadalla, A., Farag, A., Moscariello, A., 2022a. Organic geochemistry and oil-source rock correlation of the Cretaceous succession in West Wadi El-Rayan (WWER) concession: implications for a new Cretaceous petroleum system in the north Western Desert, Egypt. J. Petrol. Sci. Eng. 219, 111071. https://doi.org/ 10.1016/j.petrol.2022.111071
- Leila, M., Loisseau, K., Moretti, I., 2022b. Controls on generation and accumulation of blended gases (CH4/H2/He) in the Neoproterozoic Amadeus Basin, Australia. Mar. Petrol. Geol. 140, 105643. https://doi.org/10.1016/j.marpetgeo.2022.105643.
- Leila, M., El Sharawy, M., Bakr, A., Mohamed, A.K., 2022c. Controls of facies distribution on reservoir quality in the Messinian incised-valley fill Abu Madi Formation in Salma delta gas field, northeastern onshore Nile Delta, Egypt. J. Nat. Gas Sci. Eng. 97, 104360. https://doi.org/10.1016/j.jngse.2021.104360.
- Leila, M., Sen, S., Ganguli, S., Moscariello, A., Abioui, M., 2023a. Integrated petrographical and petrophysical evaluation for reservoir management of the upper Miocene Qawasim sandstones in west Dikirnis, onshore nile delta, Egypt. Geoener. Sci. Eng. 226, 211789. https://doi.org/10.1016/j.geoen.2023.211789.
- Leila, M., Moscariello, A., Sweet, D., Segvic, B., 2023b. Diagenetic signatures in the deltaic and fluvial-estuarine Messinian sandstone reservoirs in the Nile Delta as a tool for high-resolution stratigraphic correlations. Int. J. Sediment Res. 38, 754–768. https://doi.org/10.1016/j.ijsrc.2023.05.002.
- 754–768. https://doi.org/10.1016/j.ijsrc.2023.05.002.
  Loegering, M.J., Milkov, A.V., 2017. Geochemistry of petroleum gases and liquids from the Inhassoro, Pande and Temane fields onshore Mozambique. Geosciences 7 (2), 33. https://doi.org/10.3390/geosciences7020033.
- Lofi, J., Sage, F., Deverchere, J., Loncke, L., Maillard, A., Gaullier, V., Thinon, I., Gillet, H., Guennoc, P., Gorini, C., 2011a. Refining our knowledge of the Messinian salinity crisis records in the offshore domain through multi-site seismic analysis. La Soc. Geol. Fr 182, 163–180. https://doi.org/10.2113/gssgfbull.182.2.163.
- Lofi, J., Deverchere, J., Gaullier, V., Gillet, H., Guennoc, P., Gorini, C., Loncke, L., Maillard, A., Sage, F., Thinon, I., 2011b. Seismic Atlas of the "Messinian Salinity Crisis" Markers in the Mediterranean and Black Seas. Geological French Society, World Geological Map Commission, Paris, France, p. 72. https://ccgm.org/en/product/seismic-atlas-of-the-messinian-salinity-crisis-markers-in-the-mediterranean-sea-vol-2/.
- Lowe, D.R., 1982. Sediment gravity flows: II depositional models with special reference to the deposits of high-density turbidity current. J. Sediment. Petrol. 52, 279–297. https://doi.org/10.1306/212F7F31-2B24-11D7-8648000102C1865D.
- Mackenzie, A.S., Quigley, T.M., 1988. Principles of geochemical prospect appraisal. AAPG Bull. 72 (4), 399–415. https://doi.org/10.1306/703C8EA2-1707-11D7-8645000102C1865D.
- Madof, A.S., Bertoni, C., Lofi, J., 2019. Discovery of vast fluvial deposits provides evidence for drawdown during the late Miocene Messinian salinity crisis. Geology 47 (1), 171–174. https://doi.org/10.1130/G45873.
- Masalmeh, S.K., Wei, L., Hillgartner, H., Al-Mjeni, R., Blom, C., 2012. Developing high resolution static and dynamic models for water-flood history matching and EOR evaluation of a Middle Eastern carbonate reservoir. In: Paper SPE 161485, Abu Dhabi International Petroleum Exhibition, Abu Dhabi, UAE. https://doi.org/ 10.2118/161485-MS.
- Milkov, A.V., Etiope, G., 2018. Revised genetic diagrams for natural gases based on a global dataset of> 20,000 samples. Org. Geochem. 125, 109–120. https://doi.org/10.1016/j.orggeochem.2018.09.002.
- Mokhtar, M., Saad, M., Selim, S., 2016. Reservoir architecture of deep marine slope channel, Scarab field, offshore Nile Delta, Egypt: application of reservoir characterization. Egy. J. Petrol. 25, 495–508. https://doi.org/10.1016/ i.eipe.2015.11.003.
- Moldowan, J.M., Seifert, W.K., Arnold, E., Clardy, J., 1984. Structure proof and significance of stereoisomeric 28, 30-bisnorhopanes in petroleum and petroleum source rocks. Geochem. Cosmochim. Acta 48 (8), 1651–1661. https://doi.org/10.1016/0016-7037(84)90334-X.
- Mosconi, A., Rebora, A., Venturino, G., Bocca, P., 1996. Egypt-Nile Delta and North Sinai Cenozoic tectonic evolutionary model-A proposal. In: 58<sup>th</sup> EAGE Conference and Exhibition (Cp-48). EAGE Publications BV. https://doi.org/10.3997/2214-4609.201409027.
- Nabawy, B.S., Basal, A.M.K., Sarhan, M.A., Safa, M., 2018. Reservoir zonation, rock typing and compartmentalization of the tortonian-serravallian sequence, Temsah gas field, offshore nile delta, Egypt. Mar. Petrol. Geol. 92, 609–631. https://doi.org/10.1016/j.marpetgeo.2018.03.030.
- Nabawy, B.S., Shehata, A.M., 2015. Integrated petrophysical and geological characterization for the Sidi salem-wakar sandstones, off-shore nile delta, Egypt. J. Afr. Earth Sci. 110, 160–175. https://doi.org/10.1016/j.jafrearsci.2015.06.017.
- Nabawy, B.S., Mostafa, A., Radwan, A.A., Kotb, A.G., Leila, M., 2023. Seismic reservoir

characterization of the syn-rift lower Miocene Rudeis Formation in the July oilfield, Gulf of Suez basin, Egypt: implication for reservoir quality assessment. Geoener. Sci. Eng. 226, 211797. https://doi.org/10.1016/j.geoen.2023.211797.

- Peters, E.K., Walters, C.C., Moldowan, M.J., 2005. The Biomarker guide. In: Biomarkers and Isotopes in the Environment and Human History), second ed. Cambridge University Press, Cambridge, p. 471. https://doi.org/10.1017/CR09780511524868
- Peters, K.E., Cassa, M.R., 1994. Applied source rock geochemistry. In: Magoon, L.B., Dow, W.G. (Eds.), The Petroleum System. From Source to Trap. AAPG, Tulsa, Oklahoma, pp. 93–120. https://doi.org/10.1306/M60585C5.
- Peters, K.E., Moldowan, J.M., 1993. The biomarker guide. Interpreting Molecular Fossils in Petroleum and Ancient Sediments. Prentice Hall, Englewood Cliffs, NJ, p. 363, 1993. ISBN 0-13-086752-7.
- Pickett, G.R., 1972. Practical Formation Evaluation. Golden Colorado. GR Pickett Inc. https://search.worldcat.org/title/Practical-formation-evaluation/oclc/46707681.
- Poupon, A., Clavier, C., Dumanoir, J., Gaymard, R., Misk, A., 1970. Log analysis of sand-shale sequences-A systematic approach. J. Petrol. Technol. 22 (7), 867–881. https://doi.org/10.2118/2897-PA.
- Prinzhofer, A., Battani, A., 2003. Gas isotopes tracing: an important tool for hydrocarbon exploration. Oil & Gas Sci. Tech.-Rev. IFP 58, 299–311.
- Radwan, A.A., Abdelwahhab, M.A., Nabawy, B.S., Mahfouz, K., Ahmed, M., 2022a. Facies analysis-constrained geophysical 3D-static reservoir modeling of Cenomanian units in the Aghar Oilfield (Western Desert, Egypt): insights into paleoenvironment and petroleum geology of fluviomarine systems. Mar. Petrol. Geol. 136, 105436, https://doi.org/10.1016/j.marnetgeo.2021.105436
- Geol. 136, 105436. https://doi.org/10.1016/j.marpetgeo.2021.105436.
  Radwan, A.A., Nabawy, B.S., 2022. Hydrocarbon prospectivity of the Miocene-Pliocene clastic reservoirs, Northern Taranaki basin, New Zealand: integration of petrographic and geophysical studies. J. Pet. Explor. Prod. Technol. 12 (7), 1945–1962. https://doi.org/10.1007/s13202-021-01451-4.
- 1945—1962. https://doi.org/10.1007/s13202-021-01451-4.
  Radwan, A.A., Nabawy, B.S., Abdelmaksoud, A., Lashin, A., 2021. Integrated sedimentological and petrophysical characterization for clastic reservoirs: a case study from New Zealand. J. Nat. Gas Sci. Eng. 88, 103797. https://doi.org/10.1016/i.ingse.2021.103797.
- Radwan, A.A., Nabawy, B.S., Shihata, M., Leila, M., 2022b. Seismic interpretation, reservoir characterization, gas origin and entrapment of the Miocene-Pliocene Mangaa C sandstone, Karewa gas field, north Taranaki Basin, New Zealand. Mar. Petrol. Geol. 135, 105420. https://doi.org/10.1016/j.marpetgeo.2021.105420.
- Riad, S., Abdelrahman, E., Refai, E., El-Ghalban, H., 1989. Geothermal studied in the nile delta. J. Afr. Earth Sci. 9, 637–649. https://doi.org/10.1016/0899-5362(89)
- Rizzini, A., Vezzani, F., Cococcetta, V., Milad, G., 1978. Stratigraphy and sedimentation of a neogene—quaternary section in the nile delta area (ARE). Mar. Geol. 27 (3–4), 327–348. https://doi.org/10.1016/0025-3227(78)90038-5.
- Rogers, R., 2015. Offshore Gas Hydrates: Origins, Development, and Production. Gulf Professional Publishing, p. 381. https://doi.org/10.1016/C2014-0-02709-8.
- Roy, S., Hovland, M., Braathen, A., 2016. Evidence of fluid seepage in Grønfjorden, Spitsbergen: implications from an integrated acoustic study of seafloor morphology, marine sediments and tectonics. Mar. Geol. 380, 67–78. https:// doi.org/10.1016/j.margeo.2016.07.002.
- Said, R., 1990. The Geology of Egypt. A. Balkema Publishers, USA, p. 734. https://doi.org/10.1017/S0016756800019828.
- Sarhan, M., Hemdan, K., 1994. North Nile Delta structural setting trapping and mechanism, Egypt. 13<sup>th</sup> EGPC Expl. Prod. Conf. 1, 1–18. Cairo, Egypt.
- Sassen, R., Joye, S., Sweet, S.T., DeFreitas, D., Milkov, A., MacDonald, I., 1999. Thermogenic gas hydrates and hydrocarbon gases in complex chemosynthetic communities, Gulf of Mexico continental slope. Org. Geochem. 30 (7), 485–497. https://doi.org/10.1016/S0146-6380(99)00050-9.
- Schlumberger, 1991. Log Interpretation Principles/applications. Sugar Land.

- Schlumberger Educational Services, Texas, p. 226. https://www.slb.com/resource-library/book/log-interpretation-principles-applications.
- Schoell, M., 1983. Genetic characterization of natural gases. AAPG Bull. 67 (12), 2225–2238. https://doi.org/10.1306/AD46094A-16F7-11D7-8645000102C1865D.
- Sestini, G., 1989. Nile Delta: depositional environments and geological history. In: Pickering, K., Whateley, T. (Eds.), Deltas: Sites and Traps for Fossil Fuel, vol. 41. Geol. Soc. London Spec. Publ., London, pp. 99–128. https://doi.org/10.1144/GSL.SP.1989.041.01.0.
- Shanmugam, G., 1985. Significance of coniferous rain forests and related organic matter in generating commercial quantities of oil, Gippsland Basin, Australia. AAPG Bull. 69, 1241–1254. https://doi.org/10.1306/AD462BC3-16F7-11D7-8645000102C1865D.
- Sharaf, L., 2003. Source rock evaluation and geochemistry of condensates and natural gasses, offshore Nile Delta, Egypt. J. Petrol. Geol. 26 (2), 189–209. https://doi.org/10.1111/j.1747-5457.2003.tb00025.x.
- Skalinski, M., Kenter, J.A., 2015. Carbonate petrophysical rock typing: integrating geological attributes and petrophysical properties while linking with dynamic behaviour. Geol. Soc. London, Spec. Publ. 406 (1), 229–259. https://doi.org/ 10.1144/SP406.6.
- Schön, J., 1996. Physical Properties of Rocks: Fundamentals and Principles of Petrophysics. Elsevier, Oxford, p. 582.
- Sofer, Z., 1984. Stable carbon isotope compositions of crude oils: application to source depositional environments and petroleum alteration. AAPG Bull. 68 (1), 31–49. https://doi.org/10.1306/AD460963-16F7-11D7-8645000102C1865D.
- 31–49. https://doi.org/10.1306/AD460963-16F7-11D7-8645000102C1865D.
  Sun, Q., Wu, S., Hovland, M., Luo, P., Lu, Y., Qu, T., 2011. The morphologies and genesis of mega-pockmarks near the Xisha Uplift, South China Sea. Mar. Petrol. Geol. 28 (6), 1146–1156. https://doi.org/10.1016/j.marpetgeo.2011.03.003.
- Tiab, D., Donaldson, E.C., 2015. Petrophysics: Theory and Practice of Measuring Reservoir Rock and Fluid Transport Properties, fourth ed. Gulf Professional Publishing, Houston, p. 894. https://doi.org/10.1016/C2014-0-03707-0.
- Tissot, B.P., Welte, D.H., 1984. Petroleum Formation and Occurrence, second ed. Springer-Verlag, Berlin, p. 699. https://doi.org/10.1007/978-3-642-87813-8. Tissot, B.P., Pelet, R., Ungerer, P.H., 1987. Thermal history of sedimentary basins,
- Tissot, B.P., Pelet, R., Ungerer, P.H., 1987. Thermal history of sedimentary basins, maturation indices, and kinetics of oil and gas generation. AAPG Bull. 71 (12), 1445–1466. https://doi.org/10.1306/703C80E7-1707-11D7-8645000102C1865D
- Ungerer, P., Bessis, F., Chenet, P.Y., Durand, B., Nogaret, E., Chiarelli, A., Oudin, J., Perrin, J., 1984. Geological and Geochemical Models in Oil Exploration; Principles and Practical Examples, vol. 35. AAPG Mem, pp. 53–77. https://doi.org/ 10.1306/M35439C5.
- Vandré, C., Cramer, B., Gerling, P., Winsemann, J., 2007. Natural gas formation in the western Nile delta (Eastern Mediterranean): thermogenic versus microbial. Org. Geochem. 38 (4), 523–539. https://doi.org/10.1016/j.orggeochem.2006.12.006.
- Whiticar, M.J., 1999. Carbon and hydrogen isotope systematics of bacterial formation and oxidation of methane. Chem. Geol. 161, 291–314. https://doi.org/10.1016/S0009-2541(99)00092-3.
- Wu, X., Liu, G., Liu, Q., Liu, J., Yuan, X., 2016. Geochemical characteristics and genetic types of natural gas in the changxing-Feixianguan formations from the Yuanba gas field in the Sichuan basin, China. J. Nat. Gas Geosci. 1 (4), 267–275. https://doi.org/10.1016/j.jnggs.2016.09.003.
- Yasser, A., Leila, M., El Bastawesy, M., El Mahmoudi, A., 2022. Reservoir heterogeneity analysis and flow unit characteristics of the upper cretaceous bahariya formation in salam field, north western desert, Egypt. Arabian J. Geosci. 14, 1635. https://doi.org/10.1007/s12517-021-07985-5.
- Zein El Din, M., Matbouly, S., Moussa, S., et al., 1990. Geochemistry and oil-oil correlation in the western desert, Egypt. 12th Expl. Prod. Conf., Cairo, Egypt, pp. 107–137.